REPORT DOCUMENTATION PAGE

Form Approved OMB NO. 0704-0188

1. REPORT DATE (DD-MM-YYYY)	2. REPORT TYPE	3. DATES COVERED (From - To)
06-04-2015	Final Report	1-Sep-2013 - 31-Dec-2014

4. TITLE AND SUBTITLE

Final Report: ARO SPECIAL PROGRAMS; DOD-DARPA: Multiple Time Series Node Synchronization Utilizing Ambient Reference

5a. CONTRACT NUMBER
W911NF-13-1-0414

5b. GRANT NUMBER

5c. PROGRAM ELEMENT NUMBER

6. AUTHORS
SHEAN PHELPS, ALESSIO MEDDA

5d. PROJECT NUMBER

5e. TASK NUMBER

5f. WORK UNIT NUMBER

7. PERFORMING ORGANIZATION NAMES AND ADDRESSES

Georgia Tech Applied Research Corporatior
505 Tenth St., NW

Atlanta, GA 30332 -0001

8. PERFORMING ORGANIZATION REPORT NUMBER

9. SPONSORING/MONITORING AGENCY NAME(S) AND ADDRESS (ES)

U.S. Army Research Office
P.O. Box 12211
Research Triangle Park, NC 27709-2211

10. SPONSOR/MONITOR'S ACRONYM(S)
ARO

11. SPONSOR/MONITOR'S REPORT NUMBER(S)
64566-LS.2

12. DISTRIBUTION AVAILIBILITY STATEMENT

Approved for Public Release; Distribution Unlimited

13. SUPPLEMENTARY NOTES

The views, opinions and/or findings contained in this report are those of the author(s) and should not contrued as an official Department of the Army position, policy or decision, unless so designated by other documentation.

14. ABSTRACT

Special Operators, like professional athletes, must maintain peak physical performance in and out of training, and like professional athletes, they could benefit from having real time biometric data used to improve training and performance. In professional sports, the use of wearable sensor networks may be soon became commonplace in gathering training data for performance evaluation, but the same is not true for Special Operators, because of their specialized and exclusive training, and the demanding operational conditions. One major requirement for meaningful data analysis and collective signal processing targeted to performance assessment, is the need for fine

15. SUBJECT TERMS

BIOCHRONICITY, MULTIPLE TIME SERIES NODE SYNCHRONIZATION, SPATIOTEMPORAL CLOCK SIGNATURES, BIOLOGICAL SYSTEMS, PREDICTIVE ALGORITHMS, SPECIAL OPERATIONS

16. SECURITY CLASSIFICATION OF:			17. LIMITATION OF ABSTRACT	15. NUMBER OF PAGES	19a. NAME OF RESPONSIBLE PERSON
a. REPORT	b. ABSTRACT	c. THIS PAGE			Shean Phelps
UU	UU	UU	UU		19b. TELEPHONE NUMBER 404-407-8120

Report Title

Final Report: ARO SPECIAL PROGRAMS; DOD-DARPA: Multiple Time Series Node Synchronization Utilizing Ambient Reference

ABSTRACT

Special Operators, like professional athletes, must maintain peak physical performance in and out of training, and like professional athletes, they could benefit from having real time biometric data used to improve training and performance. In professional sports, the use of wearable sensor networks may be soon became commonplace in gathering training data for performance evaluation, but the same is not true for Special Operators, because of their specialized and exclusive training, and the demanding operational conditions. One major requirement for meaningful data analysis and collective signal processing targeted to performance assessment, is the need for fine scale synchronization among communicating nodes and across multiple domains. The severe requirements that Special Operators have to obey do not allow for common synchronization techniques, such as those that rely on a global clock. For this reason, techniques that rely on a different synchronization mechanism could potentially be implemented into a practical solution to provide real-time feedback data during training or in field operations. This final report summarizes: 1) the development of a set of Naive Bayes classification algorithms with their application to a validated (PAMAP2 dataset), 2) development of a generic analog sensor node capable of acquiring physiological data for analysis, and 3)
implementation of a Data Explorer and Labeling GUI to enable comparison and temporal alignment of extracted features of interest.

Enter List of papers submitted or published that acknowledge ARO support from the start of the project to the date of this printing. List the papers, including journal references, in the following categories:

(a) Papers published in peer-reviewed journals (N/A for none)

Received Paper

TOTAL:

Number of Papers published in peer-reviewed journals:

(b) Papers published in non-peer-reviewed journals (N/A for none)

Received Paper

TOTAL:

Number of Papers published in non peer-reviewed journals:

(c) Presentations

Number of Presentations: 0.00

Non Peer-Reviewed Conference Proceeding publications (other than abstracts):

Received	Paper

TOTAL:

Number of Non Peer-Reviewed Conference Proceeding publications (other than abstracts):

Peer-Reviewed Conference Proceeding publications (other than abstracts):

Received	Paper	
04/06/2015	1.00	Alessio Medda, Andrew Vaughan, Brian Liu, Shean Phelps. Activity Recognition using Statistical Gait Parameters from a Single Accelerometer, 2014 Asilomar Conference on Signals, Systems, and Computers (May 2014). 01-MAY-14, . : ,

TOTAL: **1**

Number of Peer-Reviewed Conference Proceeding publications (other than abstracts):

(d) Manuscripts

Received	Paper

TOTAL:

Number of Manuscripts:

Books

Received Book

TOTAL:

Received Book Chapter

TOTAL:

Patents Submitted

Patents Awarded

Awards

Graduate Students

NAME	PERCENT_SUPPORTED

FTE Equivalent:
Total Number:

Names of Post Doctorates

NAME	PERCENT_SUPPORTED

FTE Equivalent:
Total Number:

Names of Faculty Supported

NAME	PERCENT_SUPPORTED	National Academy Member
Alessio Medda	0.50	No
Brian Liu	0.05	
Shean Phelps	0.01	
FTE Equivalent:	**0.56**	
Total Number:	**3**	

Names of Under Graduate students supported

NAME	PERCENT_SUPPORTED	Discipline
Adam Szaruga	0.15	Computer and Computational Sciences
FTE Equivalent:	**0.15**	
Total Number:	**1**	

Student Metrics

This section only applies to graduating undergraduates supported by this agreement in this reporting period

The number of undergraduates funded by this agreement who graduated during this period: 0.00

The number of undergraduates funded by this agreement who graduated during this period with a degree in science, mathematics, engineering, or technology fields:..... 1.00

The number of undergraduates funded by your agreement who graduated during this period and will continue to pursue a graduate or Ph.D. degree in science, mathematics, engineering, or technology fields:..... 1.00

Number of graduating undergraduates who achieved a 3.5 GPA to 4.0 (4.0 max scale):..... 1.00

Number of graduating undergraduates funded by a DoD funded Center of Excellence grant for Education, Research and Engineering:..... 0.00

The number of undergraduates funded by your agreement who graduated during this period and intend to work for the Department of Defense 0.00

The number of undergraduates funded by your agreement who graduated during this period and will receive scholarships or fellowships for further studies in science, mathematics, engineering or technology fields:..... 0.00

Names of Personnel receiving masters degrees

NAME
Total Number:

Names of personnel receiving PHDs

NAME
Total Number:

Names of other research staff

NAME	PERCENT_SUPPORTED
FTE Equivalent:	
Total Number:	

Sub Contractors (DD882)

Inventions (DD882)

Scientific Progress

During the performing period, the following products were developed:
-A functional analog sensor node prototype with the capabilities to acquire acceleration, quaternions and electrocardiography signals (ECG).
-A set of tools for the interface and the streaming/download of the sensor node data
-A set of algorithm for the analysis of cross-domain biometric data, consisting of the following components:
  -Preprocessing and normalization
  -Feature extraction
  -Statistical signal modeling
  -Validation and comparison
Moreover, to facilitate data collection and hardware prototyping the following instrumentation and materiel were acquired:
-A Shimmer Sensing laboratory-grade wearable data acquisition system
-A National Instruments high-speed synchronous data acquisition system
-All parts and components necessary to the realization of the prototype sensor node

The selection of a high quality laboratory-grade sensor system for the acquisition of multiple physiological parameters was important for the characterization of the reference dictionary dataset. The research team evaluated several currently available systems and based its decision on several
factors; some of the most important were the following:
1) Accessibility to data;
2) Flexibility of parameters;
3) Number and type of supported sensors;
4) Integration with other developing environments (C, C++, Matlab, Java);
5) Quality, compactness, maturity;
6) Cost.

During the duration of the project, the following datasets were acquired and/or analyzed:
-Open public PAMPA2 daily activity dataset
-PhysioNet.org ECG activity dataset for normal conditions
-Mixed activity dataset acquired in laboratory settings using the Shimmer sensors

All the programming, analysis, and algorithm development was done in Matlab®, and the sensor node firmware was developed using MS Visual Studio Tools.
Because of time constraints in the development and implementation of the sensor node, no controlled data useful for the project was acquired using the hardware prototype.

Gaussian modeling and classification was also applied to data acquired in the laboratory for controlled conditions. For this purpose, the Shimmer wearable sensor system was employed, and data from three locations on the body were collected to match the same locations of the PAMAP2 data. Here, data was acquired at a high sampling rate of 512Hz. The researchers wearing the system
were then instructed to complete a routine that comprised of a preparation and warming up session, walking at a moderate pace, running at a medium pace followed by a cooling down phase. The exercise is always completed by three jumps, representing a common denominator for the data. This was done because datasets were not synchronize among each other and there was the need to
mark clearly the end of the exercise routine. Acceleration and rotational velocity was acquired at each node, and each node acquired data independently of each other; ECG was acquired by the chest sensor. Acceleration traces were recorded at the chest with extracts of low and high intensity activity displayed.

Algorithm development and code generation was entirely done in Matlab4, and was organized in three main use-case scenarios:
-Model Training
-Model Evaluation
-Model Comparison

Technology Transfer

Georgia Tech Research Institute

BIOCHRONICITY

Final Report

Period Covered by the Report

October 2013 through December 2014

Date of Report:	**December 31, 2014**
Project Title:	**Multiple Time Series Node Synchronization Utilizing Ambient Reference**
Contract Number:	**W911NF-13-1-0414**
Total Dollar Value:	**$600,023**
Program Manager:	**Dr. Jim Gimlet, Ph.D., Defense Advanced Research Projects Agency, Defense Science Office**

Submitted by:

Shean E. Phelps

Georgia Tech Research Institute
250 14th Street NW
Atlanta, GA 30080

Telephone: 404-407-8120
Fax: 404-407-9120
Email: shean.phelps@gtri.gatech.edu

Security Classification – Unclassified

Do not mark document as confidential or business proprietary.

Distribution List and Addresses

One report to:

- Dr. Jim Gimlett, james.gimlett@darpa.mil
  Defense Advanced Research Projects Agency
  Defense Sciences Office
  3701 N. Fairfax Drive
  Arlington, VA 22203-1714

Cc:

- Dr. Tracy Laabs, tracy.laabs.ctr@darpa.mil
- Ms. Jessica Mickey, Jessica.mickey.ctr@darpa.mil.

TABLE OF CONTENT

LIST OF FIGURES

LIST OF TABLES

1. INTRODUCTION

1.1 Project Overview

The work reported herein was performed by the Georgia Tech Research Institute (GTRI) under contract number W911NF-13-1-0414, "Multiple Time Series Node Synchronization Utilizing Ambient Reference." The period of performance of this effort goes from 01 September 2013 to 31 December 2014. The GTRI principal investigator was Dr. Shean Phelps, while the sponsor technical contract was Dr. Micheline Strand of the U.S. Army Research Laboratory's Army Research Office (ARO). The program manager (PM) at the Defense Advanced Research Projects Agency (DARPA) was Dr. Jim Gimlett.

This grant was awarded under the broader umbrella of the DARPA's Biochronicity program, originally managed by Dr. Christian Macedonia. The program's goal was to advance the fundamental understanding of the importance of timing and synchronization in complex biological systems. The first phase of the Biochronicity program aims to identify the common spatio-temporal clock signatures in biological systems using empirically derived data. This information was then to be used to enable development of predictive algorithms for time-dependent processes. The fundamental advancements in the understanding of timing in biological systems could be apply to many fields, one of which is enhanced training of military and non-military personnel.

1.2 Project Summary

Special Operators, like professional athletes, must maintain peak physical performance in and out of training, and like professional athletes, they could benefit from having real time biometric data used to improve training and performance. In professional sports, the use of wearable sensor networks may be soon became commonplace in gathering training data for performance evaluation, but the same is not true for Special Operators, because of their specialized and exclusive training, and the demanding operational conditions. One major requirement for meaningful data analysis and collective signal processing targeted to performance assessment, is the need for fine scale synchronization among communicating nodes and across multiple domains. The severe requirements that Special Operators have to obey do not allow for common synchronization techniques, such as those that rely on a global clock. For this reason, techniques that rely on a different synchronization mechanism could potentially be implemented into a practical solution to provide real-time feedback data during training or in field operations.

The research performed under this seed grant approached the problem using a combined hardware and software approach. An analog sensor node with generic architecture was prototyped and coupled with algorithms designed to synchronize and classify multiple time series sampled at possibly unknown and/or variable rates. The sensor node works independently of location, acquires multiple data modalities, and can be ruggedized accordingly to the conditions of operation. The algorithms are based on the concepts of primitives, for which a complex activity can be decomposed in a subset of basic activities. For this work, a dictionary of basic activity was derived using a publicly available database. The problem of synchronization across different

domains was approach from a time perspective using resampling techniques, and from an event perspective using correlation-type measurements.

During the performing period, the following products were developed

- A functional analog sensor node prototype with the capabilities to acquire acceleration, quaternions and electrocardiography signals (ECG).
- A set of tools for the interface and the streaming/download of the sensor node data
- A set of algorithm for the analysis of cross-domain biometric data, consisting of the following components:
    - Preprocessing and normalization
    - Feature extraction
    - Statistical signal modeling
    - Validation and comparison

Moreover, to facilitate data collection and hardware prototyping the following instrumentation and materiel were acquired

- A Shimmer Sensing laboratory-grade wearable data acquisition system
- A National Instruments high-speed synchronous data acquisition system
- All parts and components necessary to the realization of the prototype sensor node

The selection of a high quality laboratory-grade sensor system for the acquisition of multiple physiological parameters was important for the characterization of the reference dictionary dataset. The research team evaluated several currently available systems and based its decision on several factors; some of the most important were the following: 1) Accessibility to data; 2) Flexibility of parameters; 3) Number and type of supported sensors; 4) Integration with other developing environments (C, C++, Matlab, Java); 5) Quality, compactness, maturity; 6) Cost.

During the duration of the project, the following datasets were acquired and/or analyzed

- Open public PAMPA2 daily activity dataset
- PhysioNet.org ECG activity dataset for normal conditions
- Mixed activity dataset acquired in laboratory settings using the Shimmer sensors

All the programming, analysis, and algorithm development was done in Matlab®, and the sensor node firmware was developed using MS Visual Studio Tools.

Because of time constraints in the development and implementation of the sensor node, no controlled data useful for the project was acquired using the hardware prototype.

2. MATERIALS AND METHODS

In this section, methods and procedures will be described for the algorithm, hardware prototyping and dataset analysis.

2.1 Approach and Introduction

Human activity modeling and recognition using wearable sensor network is the first step in quantifying whole body motion during activity. New sensors have the advantage to be smaller, energy efficient and more precise than past generation sensors. Moreover, multiple sensors can now be integrated in a single package creating a truly wearable sensor suite that is unobtrusive enough to be used during normal everyday activity or physical exercise. The nature of this new generation of devices makes them optimal tools for human activity research studies in multiple disciplines. For instance, in healthcare wearable sensors applications are found in the study of Parkinson's disease, in the monitoring of medical conditions for post-traumatic events, and in the study of human motion for personalized treatments. In sport applications, modern wearable sensor systems are used to quantify athletic performance and for training optimization. In the military, wearable systems are found in multiple applications, from real-time physiological heath monitoring to the assessment of injury in the battlefield.

The traditional approach in sensor-based activity recognition considers activity as a continuous motion and it is based on global features. Here, the data stream is divided into windows, and each window is processed separately. The length of the window is chosen to allow for robust feature extraction and accurate classification. Although this model works best in controlled setting and laboratory tests, real world activities are characterized by high variability and the collected signal exhibit a collective non-stationarity. For this type of signals, performance is tightly related to window length, making fixed-window techniques suboptimal.

A different approach to global features is represented by the use of statistical motion primitive models, where a dictionary is trained from a set of primitive activities and statistical models are obtained for each set. This approach is less sensitive to variations and can captures the local aspects of the activity signal.

In this work, the basic principle of motion primitive was implemented on the statistical modeling of feature sets using probability density functions. The primitive models were trained on a publically available machine learning dataset containing several representative samples of everyday activities. This dataset contained data from sensor positioned at different location on the body, for 18 distinct activities (a complete description of the dataset is presented later in the text). The data was preprocessed and representative features of motion were extract using time, frequency and statistical quantities. Because of the large size of the feature matrix, dimensionality reduction using principal component analysis was used. The statistical modeling was done using Gaussian mixture models on the vector space spanned by the principal components. A model for each activity, location and dataset available was obtained and stored in a dedicated repository. After training, the models were cross validated and used for classification. Three use-case scenarios were developed, and they are *Training*, *Evaluation* and *Comparison*. In Figure 1 is illustrated a general diagram for the processing of raw physiological data, while in Figure 2 is

illustrated the comparison of two activities. Explanation of the functionality of each block is presented later in the text.

Figure 1.Generic diagram illustrating the acquisition and processing or physiological data. The model derived from the processing is stored in a dedicated repository.

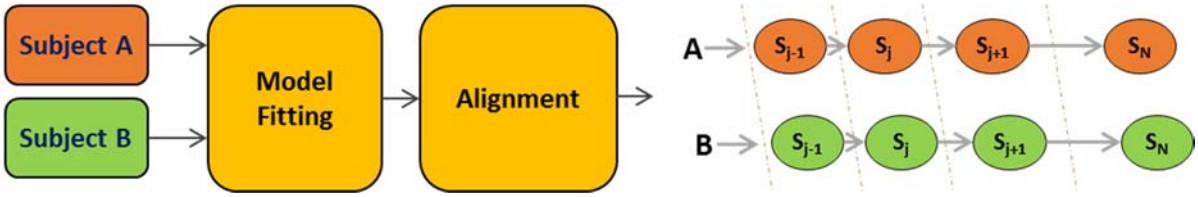

Figure 2. Generic diagram illustrating the comparison of two activities from two subjects. The result of this comparison is a chain of states describing the activity time evolution.

2.2 Datasets used for analysis

Several datasets were used throughout the duration of the project. Here, a brief summary for each one of them is presented.

PAMAP 2 dataset

The UC Irvine University Physical Activity Monitoring for Aging People II (PAMAP2) dataset was used for the analysis and model characterization of basic activities like sitting, standing, walking, running etc. The PAMAP 2 dataset was used in several peer-reviewed studies and contains a wide array of reference activities acquired for multiple subjects. In particular, the PAMAP 2 dataset contains data recorded from 9 subjects (8 males and one female, age 27.22 ± 3.31 years) and a total of 18 activities. Each participant wore three Colibri wireless inertial measurement units (IMU) sensors and one heart rate monitor (HR-monitor). Data was collected at three location on the body, at the chest, at the wrist and at the ankle. ECG was measured at the chest only using the HR-monitor. Sampling frequency was of 100 Hz for the IMUs and 9 Hz for the HR-monitor. The IMU collected acceleration at two different scales, $\pm 16g$ and $\pm 6g$, angular velocity (rad/s), magnetometer (μT) and temperature ($°C$). The HR-monitor registered heart rate in beat-per-minute (bpm). For the data collection, each participant followed a protocol containing twelve different activities. A total of 10 hours of data were collected, from which nearly 8 hours were labeled accordingly to Table I.

The activities of *Sitting (SIT)*, *Standing (STD)*, *Lying (LNG)*, *Walking (WLK)*, *Running (RUN)* and *Cycling* (CYC) were chosen for the analysis. An example of accelerometer data from these activities is shown in **Figure 3**.

Table 1– PAMPA2 DATASET ACTIVITIES DESCRIPTION (Highlighted activities were selected for the study)

ID	Activity	Description	ID	Activity	Description
1	**Lying**	*Lying quietly, small*	**10**	**Cycling**	*Biking with real bike*
2	**Sitting**	*Sitting in a chair*	**11**	**Running**	*Jogging outside*
3	**Standing**	*Standing still*	**12**	**Rope Jumping**	*Basic jumps and alternate*
4	**Ironing**	*Ironing 1 or 2 T-Shirts*	**13**	**Watching TV**	*Watch TV at home*
5	**Vacuuming**	*Vacuum cleaning*	**14**	**Computer Work**	*Normal office work*
6	**Ascending stairs**	*Going upstairs*	**15**	**Car Driving**	*Driving normal traffic*
7	**Descending stairs**	*Going downstairs*	**16**	**Folding Laundry**	*Folding T-Shirts*
8	**Normal walking**	*Walking at moderate*	**17**	**House Cleaning**	*Dusting*
9	**Nordic walking**	*With walking poles*	**18**	**Playing Soccer**	*Running, dribbling, passing*

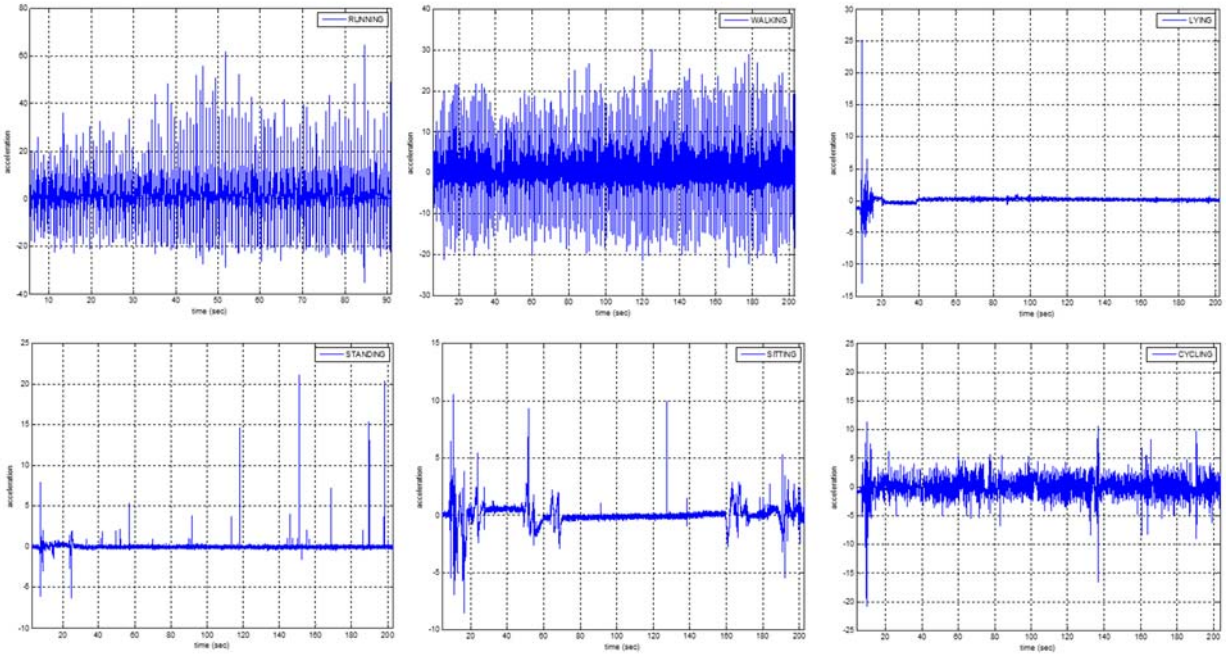

Figure 3. Example of vertical acceleration from chest mounted sensor recorded for the activities of *Walking*, *Running*, *Lying*, *Standing*, *Sitting* and *Cycling*.

PhysioNet Datasets

For the analysis of physiological data from ECG, several PhysioBank[1] dataset were investigated. The data from this repository is often used for peer-reviewed studies in the biomedical research community and it is well documented and characterized. The datasets considered from this project (listed below) were used to derive the preprocessing algorithms and the correct type of features.

- **AAMI EC13**. This dataset contains signal from 10 short recordings (60 sec) specified by the current American National Standard for testing various devices that measure heart

[1] www.physionet.erg/physiobank

rate. Each recording contains a single lead ECG sampled at 720Hz and 12 bit resolution over ±10mV.

- **MIT-BIH Arrhythmia**. This dataset contains signal from the first generally available set of standard test material for the evaluation of arrhythmia detectors. The database contains long recording (48 half-hours) from two channel ambulatory ECG from 47 subjects. Samples are recorded at 360Hz with 11-bit resolution over ±10mV.
- **BIDMC CHF**. This dataset contains long term ECG from subjects with severe congestive heart failure (CHF) conditions. Individuals recordings are about 20 hours double lead at 250Hz at 12-bit resolution over ±10mV. Original signal bandwidth is about 0.1Hz to 40Hz.
- **Fantasia**. This dataset contains 120-minute recordings of resting ECG and respiratory signals from 48 healthy subjects, digitized at 250Hz.

An example of ECG data from the MIT-BIH and AAMIec13 dataset is shown in Figure 4. In addition to ECG, photoplethysmography (PPG) was also considered at the beginning of the project, but was not included in the final data types for this study. The PPG high sensitivity to motion artifacts and the difficulties of PPG data acquisition outside of controlled settings made this measurement not a good candidate for motion classification and it was the leading factor in the decision not to consider it further into the study.

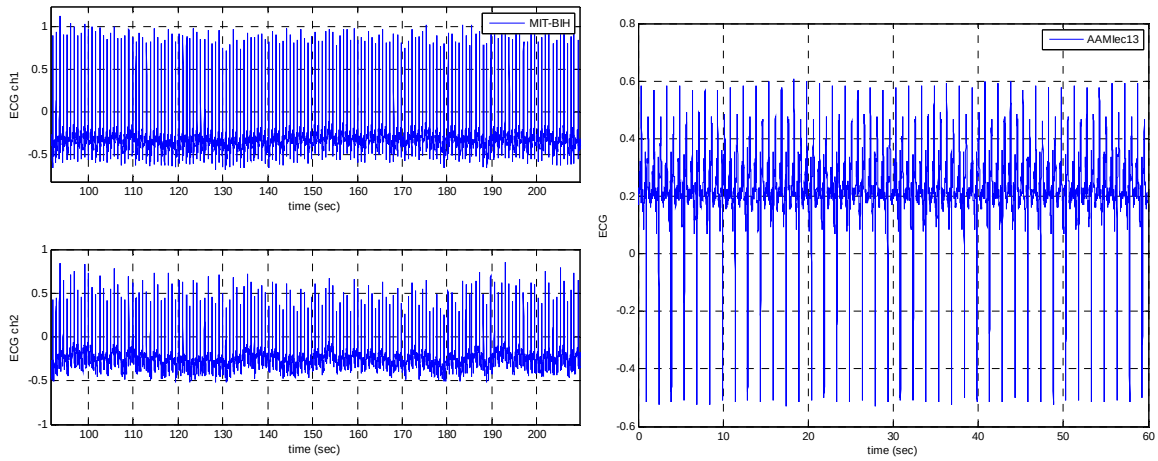

Figure 4. Example of ECG signal from dataset MIT-BIH (left) and AAMIec13 (right).

Mixed activity laboratory dataset

This dataset was acquired using the Shimmer Sensing wearable data acquisition system. Because the Shimmer system is modular and allows wireless communication between a base station and the sensors, a diversified set of sensors were selected for the laboratory testing. The sensor types selected for testing are accelerometer, ECG, and 9DoF IMU. Moreover, this system integrates a high quality triaxial accelerometer in every sensor, eliminating the need for adding standalone sensors.

For this dataset, volunteers from GTRI laboratory were instrumented with a chest, ankle and arm Shimmer sensor and instructed to perform a complex exercise routine that consisted in an alternated session of walking-running-walking followed by three jumps. This is illustrated in the example of Figure 5, where acceleration for the vertical, lateral and horizontal direction is plotted against time. Figure 6 instead shows an example of ECG signal acquired with the Shimmer sensors at chest location. All data is acquired at the sampling rate of 512 Hz.

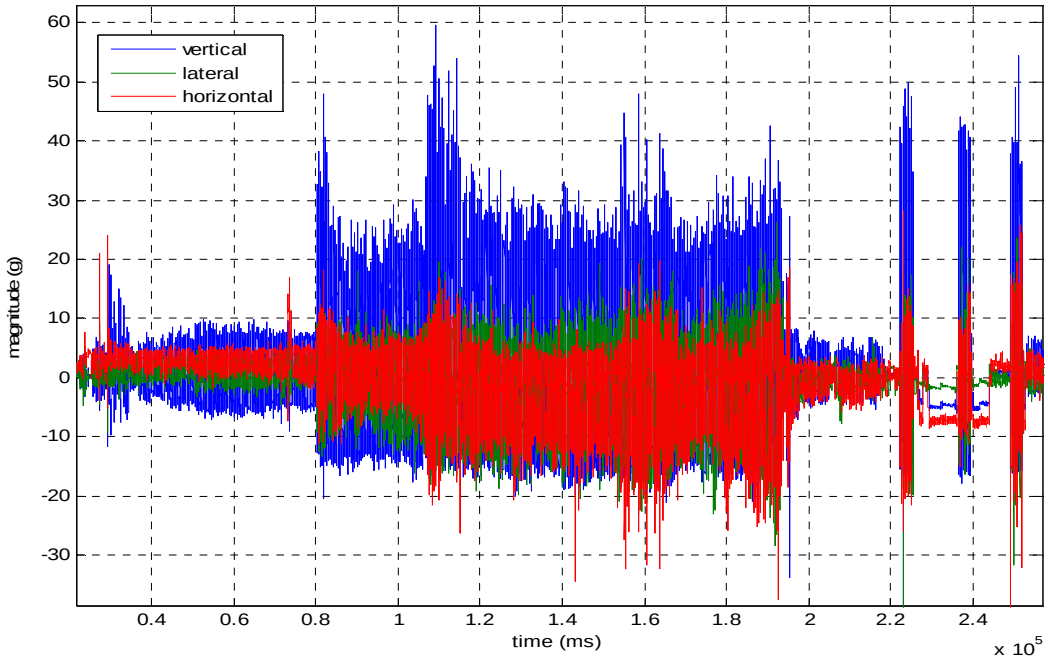

Figure 5. Example of vertical, lateral and horizontal acceleration recorded from a chest mounted Shimmer unit for a sequence of walk-run-walk exercise.

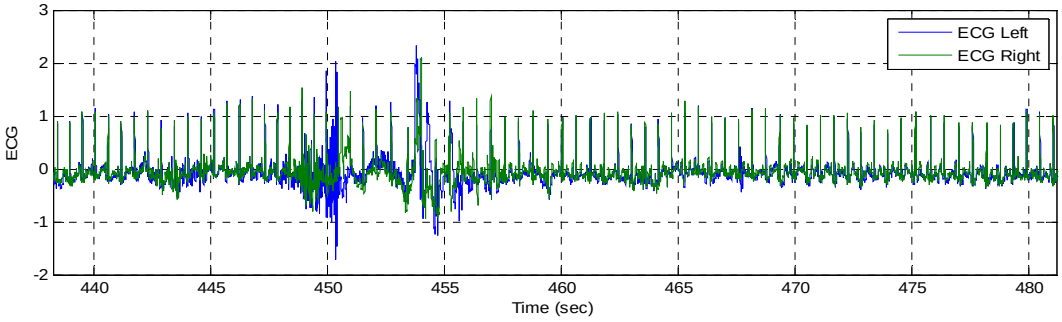

Figure 6. Example of ECG signal acquired with the Shimmer sensors at chest location.

2.3 Preprocessing

Signal preprocessing represent the first step in the analysis of the input data from the sensors and it is essential to the conditioning of the raw data for the remaining processing steps. In the

preprocessing phase, data artifacts are mitigated or eliminated, and although the applied techniques varied depending on the signal type, some operations are common to all signals. In particular, all signals received for analysis are processed to remove DC drifts and noise. Some specialized processing is required for ECG signals. The following list illustrates the preprocessing implemented for each signal type:

- **Acceleration**: detrending and denoising
- **Angular Velocity**: detrending and denoising
- **ECG**: detrending, denoising, and removal of respiration signal

Offset removal and detrending

When the trend is a constant, the DC offset of the signal can be corrected by subtracting the mean of the signal from the signal itself. This is done by selecting a stationary portion of the signal, usually starting from the first or the last sample, and computing the mean over a window. This is a good estimate of the DC offset, and it is then removed from the signal.

When signals are characterized by variable offsets, trends are estimated and removed using interpolation techniques. In this case, a low order polynomial fit is computed on the signal samples to find the best approximation to the data. Keeping the degree of the fitting polynomial low ensures that the fit approximates the general trend of the data without removing important information.

Denoising

Because sensor signals will invariantly contain noise, the process of removing or attenuating this noise is important to assure that the best quality possible. Moreover, attenuation of unwanted noise in the data is particularly important for the analysis of signals tightly correlated with the phenomenon under observation. This is because of salient features in the data that may be masked by the noise, and preserving these features guarantees good overall modeling performances.

Classical denoising techniques based on lowpass filtering rely on the assumption that the signal and the noise are separated in the frequency spectrum. In particular, it is commonly assumed that the signal is contained in the lower portion of the frequency spectrum while the noise is associated with higher frequency components. Although this assumption holds especially well in the case of localized noise components, such as frequency peaks associated with resonant frequencies, real noise is usually found over the entire Nyquist interval. In particular, any disturbance that can be model as a sequence of uncorrelated random variables with given probability distribution function follows in this category. For a Gaussian distributed discrete random variable $n(k)$, we have white Gaussian noise, which power spectrum is given by the Fourier transform of its autocovariance function $C_n(k) = \sigma_n^2 \delta(k)$, or $P_n(f) = \sigma_n^2 \ \forall f \in (\infty, \infty)$. Therefore, if signal and noise are intermixed in the frequency range of interest, lowpass filtering the signal is not a good solution for the mitigation of the noise.

An alternative approach is offered by the application of wavelet theory to signal analysis. While lowpass filtering is a form of denoising in the frequency domain alone, wavelet denoising operates in a different transformed domain. A wavelet is a basis function that is concentrated in both time and frequency, which, and unlike the Fourier transform, provides a scale dependent time-frequency

representation of a signal. The discrete wavelet transform (DWT) algorithm represents the signal using wavelets as basis functions through dilations and translations on a dyadic grid.

Let us define a discretized signal $y(k)$ and suppose that there are N samples of a function $f(t)$, such that

$$y_k = f(t_k) + \sigma_n \epsilon_k, \quad k = 1,2, \dots N \tag{1}$$

where ϵ_k are iid[2] samples for a Gaussian process with zero mean and unit variance, and σ_n represent the power of the noise. The DWT, yields the following

$$y_{jk} = w_{jk} + \sigma_n \epsilon_{jk} \tag{2}$$

where w_{jk} are the wavelet coefficient of $f(t_k)$.

The advantage of the DWT representation is that, due to linearity of the wavelet transform, the coefficients of the observed signal can themselves be considered a noisy version of the wavelet coefficients of the original signal. Also, because of the sparsity properties of the wavelet transform, the energy of the original signal is usually concentrated in few coefficients, with the rest of them being very small or close to zero. Therefore, for a signal contaminated by Gaussian noise the DWT produces a small number of coefficients with high amplitude and a larger number of small magnitude coefficients. The approach for which each coefficient is compared with a threshold to decide whether it constitutes a desirable part of the original signal or not, is called *wavelet thresholding*. The thresholding extracts the significant coefficients by setting to zero the coefficients which their absolute value is below a certain threshold level λ. An example of wavelet denoising for an impulsive signal is shown in Figure 7.

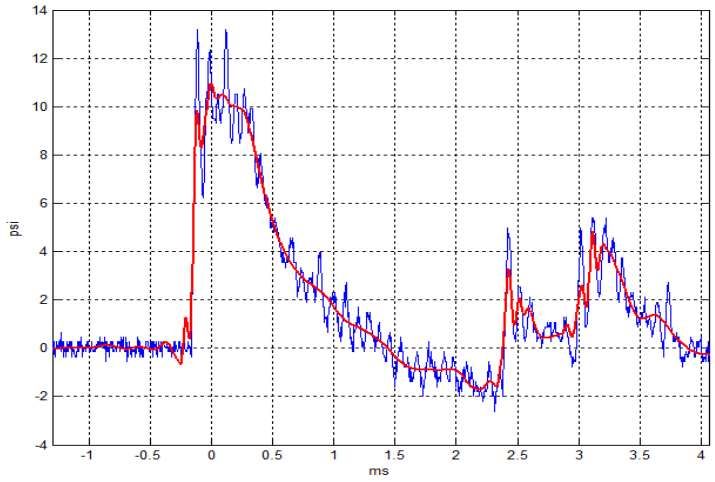

Figure 7 – Example of wavelet denoising.

[2] *iid*: independent identically distributed

ECG preprocessing

The ECG signal records the electrical activity of the heart using electrodes placed directly on the skin of the participants. The signals recorded by ECG are the voltage variations of the heart cells action potentials during contractions. The aim of preprocessing for ECG is to improve the general quality of the signals for a more accurate analysis and feature extraction, enhancing the characteristics of the QRS complex without corrupting the rest. Noise and other spurious components can distort the ECG recordings to such an extent that measurements of the QRS complexes becomes unreliable or not possible. The three main types of noise usually affecting ECG signals are

- Low frequency baseline wonder caused by respiration and body movements
- High frequency random noise cause by electrical interferences and muscular activity
- Random shifts in ECG signals caused by poor electrode contact

In literature, a classical approach for the preprocessing of ECG recordings and the detection of QRS complexes is the removal of baseline wonder and high frequency noise using an adapting filtering approach and classical denoising techniques. In this work, we chose to process the ECG using wavelet denoising for the elimination of random noise and Variational Mode Decomposition (VMD) for the mitigation of baseline wonder. Moreover, during the investigation, an adaptive filtering method based on the Least-Mean Square (LMS) algorithm and using the jointly recorded acceleration-ECG signals were implement as an alternative to VMD processing. The drawback of this approach is that need for acceleration to be recorded simultaneously to the ECG, in addition to the long converging time of the adaptive processor. For this reason, the VMD technique is the preferred method, although both techniques are presented here.

Variable Mode Decomposition (VMD)

Here, a summary of the VMD method as it was applied to the ECG signal used in this work is presented. Because of the space required fully present the VMD theory and framework, the reader is referred to the bibliography for any additional information.

The VMD method is based on the concept of Intrinsic Mode Function (IMF) and it represents an effort to extend and formalize the well-known Empirical Mode Decomposition (EMD) proposed by *Huang et al*. In the EMD method, the IMF are amplitude and frequency modulated functions of the form $m_k(t) = A_k(t)cos\big(\phi_k(t)\big)$, with instantaneous frequency defined by $f_k(t) = \phi_k{}'(t)$. Therefore, for long enough intervals, $m_k(t)$ can be considered to be a pure harmonic signal. Although the original EMD algorithm lacks a formal mathematical description and it is sensitive to noise and variations in sampling, it was used in a large number of applications in several engineering, medicine, and technology fields.

The VMD algorithm proposes an intrinsic and adaptive variational method which minimization leads to the decomposition of the signal into its principal modes. VMD determines the relevant bands adaptively, and estimates the corresponding modes concurrently, properly balancing the errors between them. The goal of the VMD method is to decompose an input signal into a discrete number of modes that have specific sparsity properties while reproducing the input. Here, it is assume each mode m_k be mostly compact around a center frequency $f_k(t)$, which is to be

determined along with the decomposition. The constraint variational problem, as described in the original work of *Dragomiretskiy and Zosso*, can be formulated as following

$$\min_{(m_k, f_k)} \left\{ \sum_k \left\| \partial_t \left[\left(\delta(t) + {}^{j}/_{\pi t} \right) * m_k(t) \right] e^{-i f_k t} \right\|_2^2 \right\}$$

such that $\sum_k m_k(t) = f(t)$. For the solution of the minimization with respect to m_k and f_k, the reader is referred to the original work cited in the bibliography.

The application to the VMD algorithm to the ECG signal produces a multi-function representation, where different components are representative of the different frequency characteristics of the ECG. Therefore, low frequency variations associated to respiration appears in lower modes (associated to low center frequencies), while high frequency noise from muscular activity and other sources appears in higher modes. It is also possible to reconstruct the original signal $f(t)$ discarding unwanted components, obtaining in this way a simplified version of $f(t)$. This is illustrated in Figure 8, where the original (red) ECG is shown together with the VMD-filtered ECG and Figure 9.

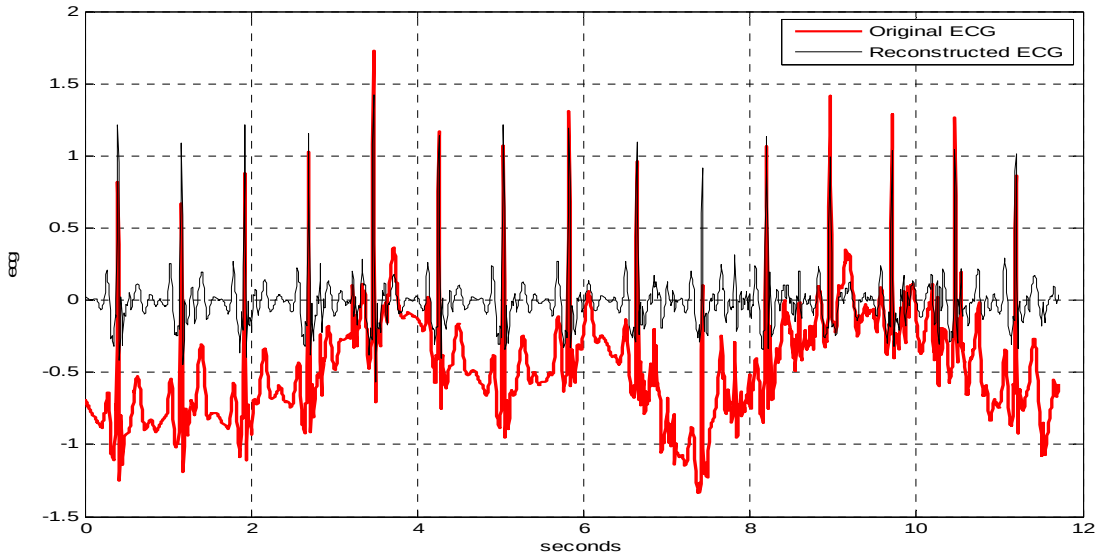

Figure 8. Example of ECG signal corrupted by low variational noise associated with respiration and movement. Here the original signal (red) is shown along with the VMD-filter one, obtained considering all but the first and last components of a six-mode decomposition.

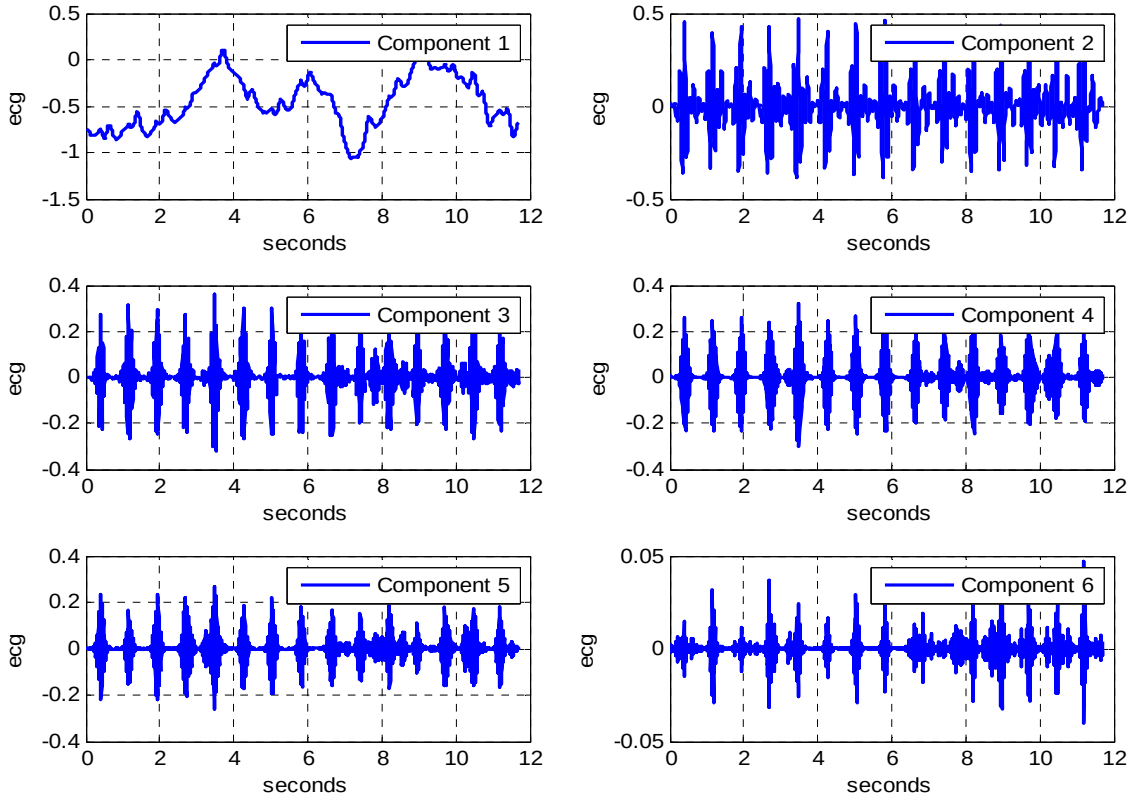

Figure 9. VMD modes obtained from the signal from Figure 8.

Least-Mean Square (LMS) filtering

Adaptive filtering was used to remove low frequency wander from respiration signal and motion artifacts associated with body motion. Acceleration from a co-located ECG/accelerometer was used in an adaptive filter to estimate motion induced artifacts of the ECG. The LMS algorithm was used for the adaptive processor. The MLS method is an iterative approach for the minimization of the mean square error (MSE) between the primary and a reference signal. An adaptive filter based on the LMS algorithm is schematically illustrated in Figure 10, where the accelerometer signal is dynamically subtracted from the ECG signal such that the MSE error is minimized. For the details on the implementation of the LMS algorithm, the reader is referred to the bibliography. Despite the only indirect correlation of the acceleration with the motion artifact corrupting the ECG, the simplicity and relative stability of the LMS algorithm produced good acceptable results, as shown in Figure 11.

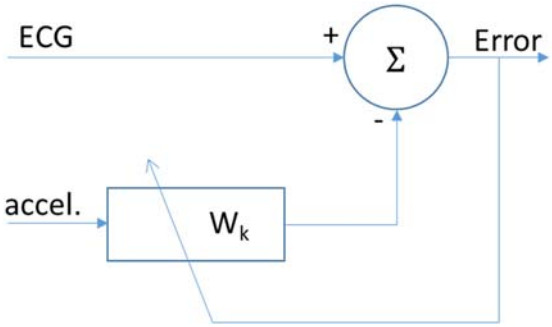

Figure 10. Schematic illustration of adaptive filter.

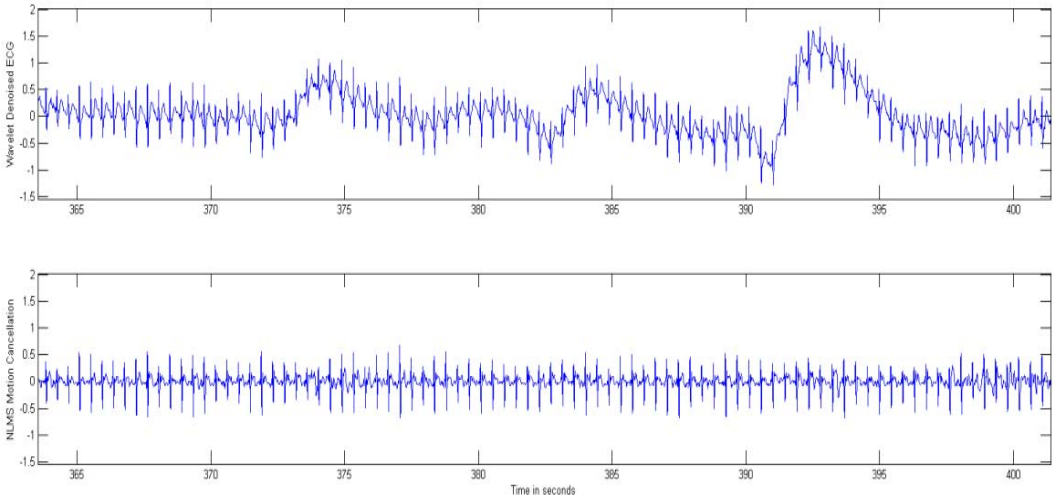

Figure 11. Example of LMS processing for the removal of low frequency wonder. Top: original ECG signal corrupted by respiration noise. Bottom: clear ECG signal after LMS filtering.

2.4 Segmentation

In case of data comprised of blocks of basic or constant activities, the developed algorithm incorporates an option to segment the data and process these segments independently. This option is important mostly when generating primitive models without bias. Each segment should be representative of a portion of the signal where variance is somehow constant.

Manual segmentation is based on user input, using custom designed interfaces to guide the user in the selection of the relevant segments. While this method allows for precise localization of the segment boundaries and it is most useful when dealing with more complex data, its usage is only realistic in an ad-hoc analysis or when the number of traces to analyze is small. During manual segmentation, the user is prompt to choose if manual segmentation is needed, and then he is presented with an interface where flexible breakpoints can be overlapped to the time trace, selecting the intervals that will define the data segments. This process is shown in Figure 12.

For large datasets, an automatic segmentation routine was developed. Two methods for the automatic segmentation of data were investigated, one based on continuous Changes in Variance (CV), and one based on the Cumulative Sum Method (CSM). The CV method looks for changing

in the variance of the signal associated with a change in physical activity. Transition times are computed at the point of variation. CSM computes the statistics of the signal for a running window and compares the log-likelihood of the distribution of the signal at the right and left of the window middle point. Examples of the results obtain using these two techniques are shown in Figure 13 and Figure 14.

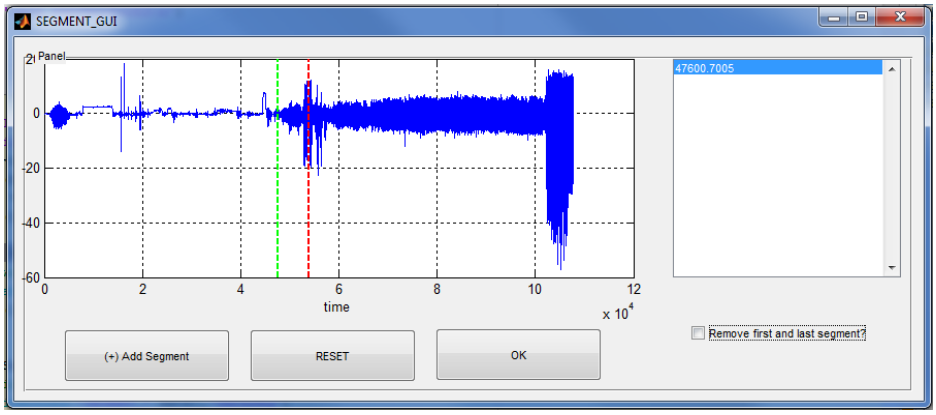

Figure 12. *Detail of the custom interface for the definition of manual segmentation breakpoints.*

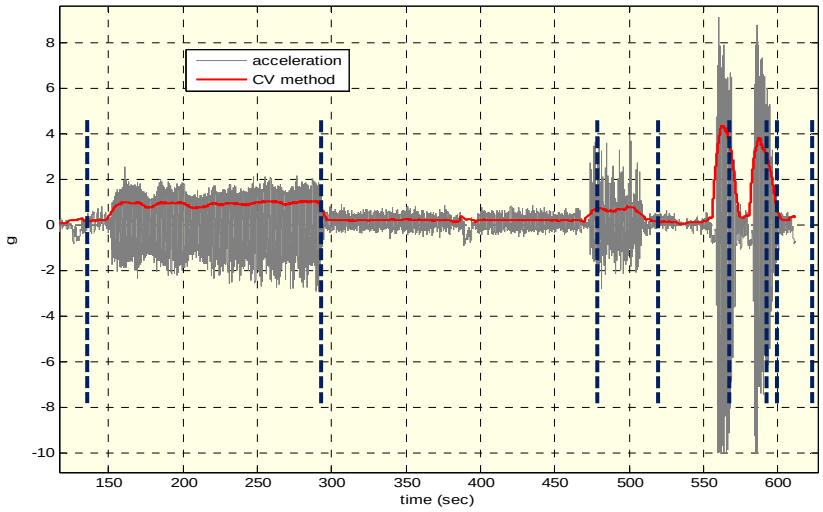

Figure 13. Example of CS method results on acceleration measured at the arm for multiple recorded physical activities. The transition points in black are manually highlighted for comparison with dashed lines.

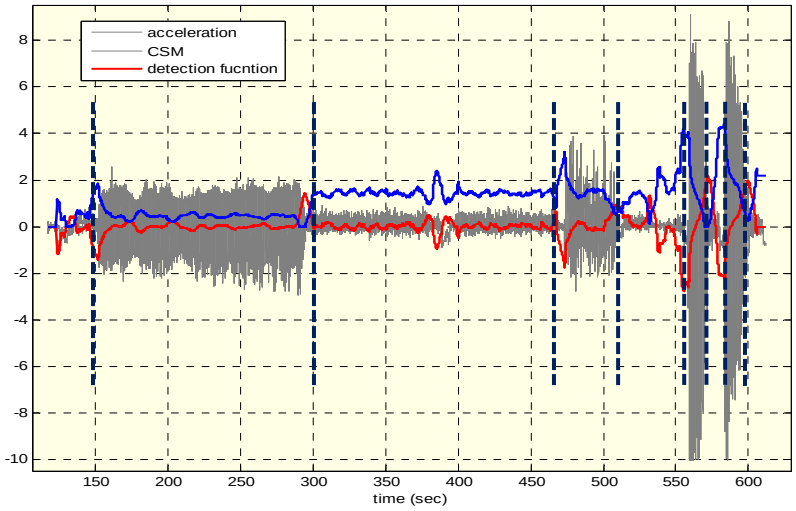

Figure 14. Example of CSM method results on acceleration measured at the arm for multiple recorded physical activities. The transition points in black are manually highlighted for comparison with dashed lines.

2.5 Feature Extraction

Features of interest were derived from the isolated segments of data and used for classification. A dimensionality reduction algorithm based on Principal Component Analysis was developed and used on the derived feature sets. Two feature extraction algorithms were developed, one for the acceleration and one for the ECG signals, both characterized by time and frequency features.

Acceleration Features

Acceleration features are computed from recorded acceleration for the x-, y-, and z-axis of the sensor reference system. Each feature is computed on a moving window, so that the resulting feature is a vector of the same length of the signal in input. The optimal length for the observability window was set to three time the sampling frequency, as determine during experimentation. This value was found to be optimal for our application, using the data provided by the PAMAP2 dataset.

The features implemented in the algorithm are the following

- Movement Intensity (MI)

$$MI[k] = \sqrt{a_x[k]^2 + a_y[k]^2 + a_z[k]^2}$$

- Mean

$$\mu_{AR} = \frac{1}{N}\sum_i MI[i]$$

- Variance

$$\sigma_{MI}{}^2 = \frac{1}{N-1}\sum_i (MI[i] - \mu_{MI})^2$$

- Skewness

$$SK_{MI}{}^2 = \frac{\frac{1}{N}\sum_i (MI[i] - \mu_{MI})^3}{\left(\sqrt{\sigma_{AR}{}^2}\right)^3}$$

- Kurtosis

$$KT_{MI}{}^2 = \frac{\frac{1}{N}\sum_i (MI[i] - \mu_{MI})^4}{(\sigma_{AR}{}^2)^2}$$

- Median of $MI[i]$
- 10th and 90th percentile of $\boldsymbol{MI}[\boldsymbol{i}]$ ($\boldsymbol{p10MI}$ and $\boldsymbol{p90MI}$)
- Dominant frequency, defined as the maximum of the power spectral density of $\boldsymbol{MI}[\boldsymbol{i}]$
- Spectral Entropy, defined as the entropy of the normalized power spectral density (PSD), and compute as

$$H = -\sum PSD \log_2 PSD$$

In addition to these basic features, two additional features were considered:

- Angle between acceleration vectors defined as

$$modulus\left[\frac{\tan^{-1}\left(\frac{a_i}{a_j}\right) - \frac{\pi}{4}}{2\pi}\right] - \pi$$

  where $(i, j) = \{x, y, z\}$ and $i \neq j$
- Derivative of the angle as computed above

ECG Features

For heart activity, one of the most effective parameter in predicting heart behavior is the heart rate variability (HRV), defined as the variation of beat-to-beat intervals in heart rate. This quantity was computed as the time difference between the peaks of QRS complexes (also called RR intervals), and provides an indirect measurement of the physiological behavior of the heart. Several indicators were derived from this measure, where the most important are detailed in Figure 15. Moreover, instantaneous heart rate (HR) is directly derived from the HRV signal. In literature, HRV was used to quantify improvement in training and fitness performance in different conditions and sport activity, and it therefore represent a valuable source of information. Figure 16 to Figure 18 show an example from a 47-minute long ECG recording using the Shimmer system, the derived HRV, HR and power spectrum.

Measure	Description	Unit
AVNN	Average of all NN intervals	ms
SDNN	Standard deviation of all NN intervals.	ms
RMSSD	The square root of the mean of the sum of the squares of differences between adjacent NN intervals	ms
pNN50	Percentage of differences between adjacent NN intervals that are > 50 ms	%
TOTPWR	Total spectral power of all NN intervals 0-0.4 Hz.	ms^2
VLF	Total spectral power of all NN intervals 0-0.04 Hz	ms^2
LF	Total spectral power of all NN intervals 0.04-0.15 Hz	ms^2
HF	Total spectral power of all NN intervals 0.15-0.4 Hz	ms^2
LF/HF	Ratio of low to high frequency power	

Figure 15 – Definition for HRV time and frequency measurements.

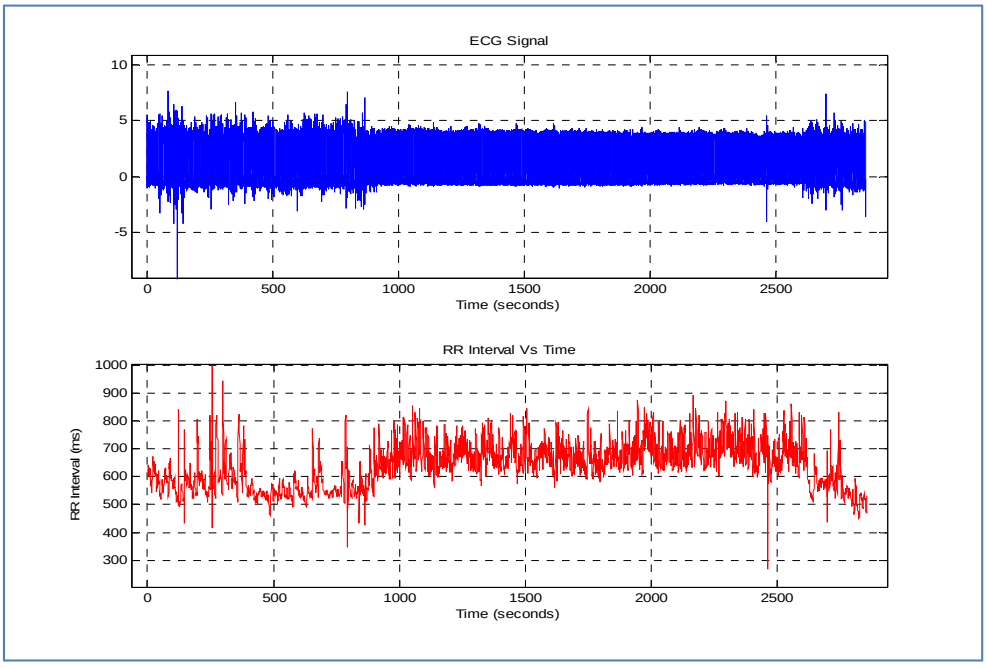

Figure 16 – (Top) ECG signal from a 47-minute long recording using the shimmer system. (Bottom) Derived HRV measure.

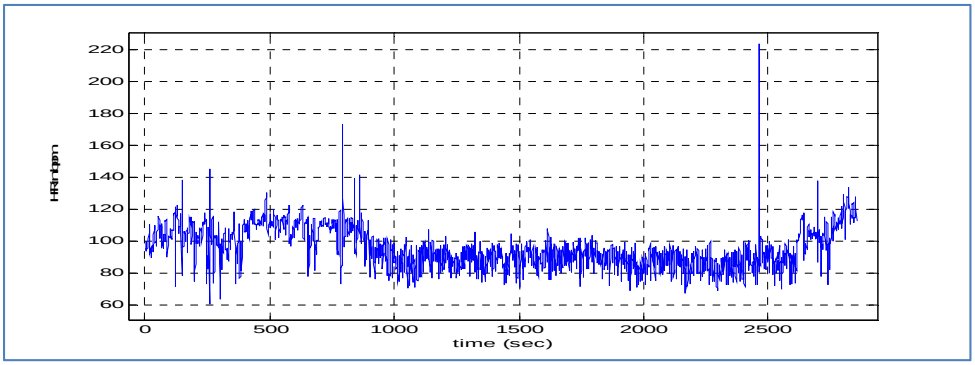

Figure 17 – Instantaneous HR computed from the HRV signal of Figure 16.

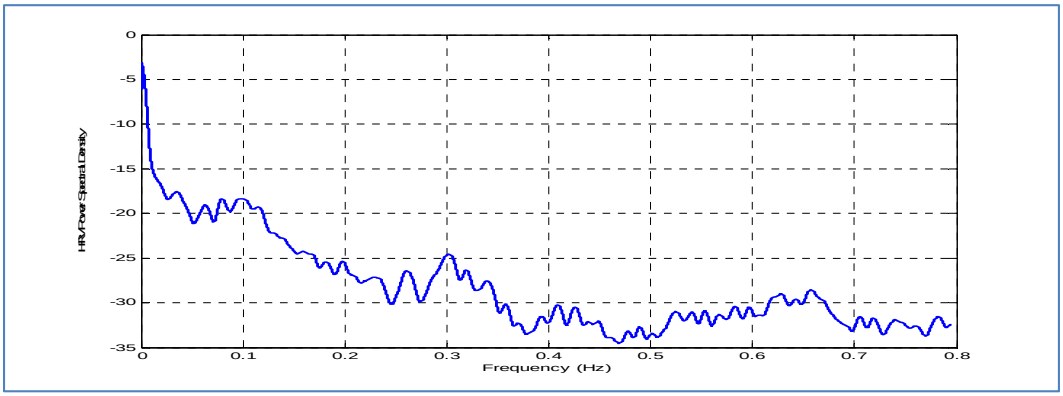

Figure 18 – Power Spectral Density from the HRV signal of Figure 16.

TABLE 2 – HRV STATISTICS COMPUTED ON THE SIGNAL FROM FIGURE 16.

Time domain measures		**Frequency domain measures**	
Mean HR	95.4 bpm	**VLF peak**	9.7 10^{-5} Hz
Std HR	12.0 bpm	**VLF abs pwr**	0.0029 s^2
AVNN	0.639 ms	**VLF rel pwr**	65%
SDNN	0.0784 ms	**LF peak**	0.04 Hz
RMSSD	0.038 ms	**LF abs pwr**	0.0011 s^2
		LF rel pwr	25%
		HF peak	0.15 Hz
		HF abs pwr	4.610^{-4} s^2
		HF rel pwr	10%
		LF/HF	2.38

2.6 Statistical Modeling

Acceleration and ECG features distributions are modelled after dimensionality reduction, keeping feature sets separated for identification. Dimensionality reduction is done using Principal Component Analysis (PCA), while the modeling of the feature densities is done using Gaussian mixture models.

Dimensionality Reduction using PCA

Principal Component Analysis (PCA) is used to concentrate the information provided by the feature vector in few components of high variance. The basic idea in the application of PCA to a is to find the component vectors $y_1, y_2, \ldots, y_N$ that explain the maximum amount of variance possible by N linearly transformed components. An intuitive way to define PCA is to use a recursive formulation. If we define the first principal component as v_1, its direction is found by the solution of the maximization problem $v_1 = \arg max_{\|V\|=1} E[(v_1^T \mathbf{X})^2]$, where v_1 is the first principal component and $\mathbf{X}$ is the vector containing the data. Therefore, v_1 is the projection of $\mathbf{X}$ in the direction that maximizes the variance. Each remaining $N-1$ components are computed by repeating this process in the remaining orthogonal subspace. The principal components are then given by

$$y_i = v_i^T \mathbf{X} \quad \forall i = 1, \ldots N$$

This operation transforms the column of X into y_i using the quantities v_i^T. These quantities can also be computed using the simple covariance matrix $\boldsymbol{C} = \mathbf{X}^T \mathbf{X}$, where the v_i are the eigenvectors of $\boldsymbol{C}$, which correspond to an equal number of eigenvalues. The transformation that from X obtains yi using the eigenvectors of the covariance matrix is also known as Karhunen-Loève transform.

In the analysis, the dimensionality of the data is reduced from N to p, where $p < N$ to remove unwanted components. This comes from the assumption that the data in the last $N-p$ components is mostly noise, therefore keeping the first p components we ensure that all signal information is represented. For our application, p is selected such as to keep at least 80% of the original signal energy. Although the number of components for which this condition is met varies with the type of activity and the measurement location, it was found that on average the first three principal components account for at least 80% of the energy. As an example, Figure *19* shows the cumulative variance for the activities of walking and running measured at the chest and ankle.

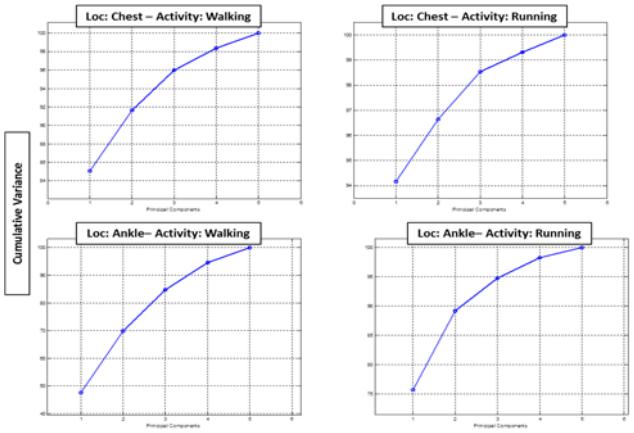

Figure 19 - Cumulative variance as function of principal component, type of activity and measurement location.

Gaussian Mixture Models

Each set of principal components is then modeled using Gaussian mixture modeling, a parametric density estimation technique. The concept of mixture modeling is based on the assumption that any continuous distribution can be approximated arbitrarily well by a finite mixture of normal densities with common variance. For a family of Gaussian distributions, and a given finite data set $\boldsymbol{X} = [x_1, x_2, \ldots\ x_N]$ of *N* observations, the approximated mixture density has the following form

$$f_{\mathrm{K}}(x;\theta) = \sum_{k=1}^{\mathrm{K}} w_k\ g(x;\theta_k)$$

with $\boldsymbol{\theta} = [w_1 \ldots w_{\mathrm{K}};\ \theta_1\ \theta_2 \ldots \theta_{\mathrm{K}}]^T$ and $\theta_k = \{\mu_k, \sigma_k\}$**.** The quantity w_k is the mixing probability of the k^{th} component of the mixture. The model parameters w_k, μ_k and σ_k need to be estimated for each one of the *K* components in the mixture, and the one-dimensional Gaussian kernel is defined as

$$g_k = g(x;\theta_k) = \frac{1}{\sqrt{2\pi}\sigma_k} e^{-\frac{(x-\mu_k)^2}{2{\sigma_k}^2}}$$

A classical solution to this problem is the use of the Expectation-Maximization (EM) algorithm, that for a finite dataset and an initial mixture $f^{(0)}$, provides a sequence of mixture models $f^{(k)}$ with increasing log-likelihood on the data. For details on the EM algorithm, see bibliography reference.

The estimation of the number of components remains a problem. When a large model order is selected, the resulting model is modeling the part of the signal associated with noise, while on the other hand if a small model order is selected, not enough parameters are provided to the model to properly represent all signal features. In this case, the model order K was estimated as an average between repetitions for minimum values of the corrected Akaike information criterion (AICc) and the Bayes Information Criterion (BIC). Here, the AICc is defined as

$$AICc = -2\mathcal{L}(\boldsymbol{x}_n, f_k) + \frac{2N(3k-1)}{N-(3k-1)-1}$$

while the BIC is defined as

$$BIC = -2\mathcal{L}(\boldsymbol{x}_n, f_k) + (3k-1)\log N$$

with $\mathcal{L}(\boldsymbol{x}_n, f_k) = \mathcal{L}_k = \sum_{m=1}^{M} \log f_k$ as the log likelihood of the estimated mixture, and f_k the k^{th} mixture component. An example of computed mixtures for $K = 3$ and two principal components is shown in Figure *20* for the activity of walking and running.

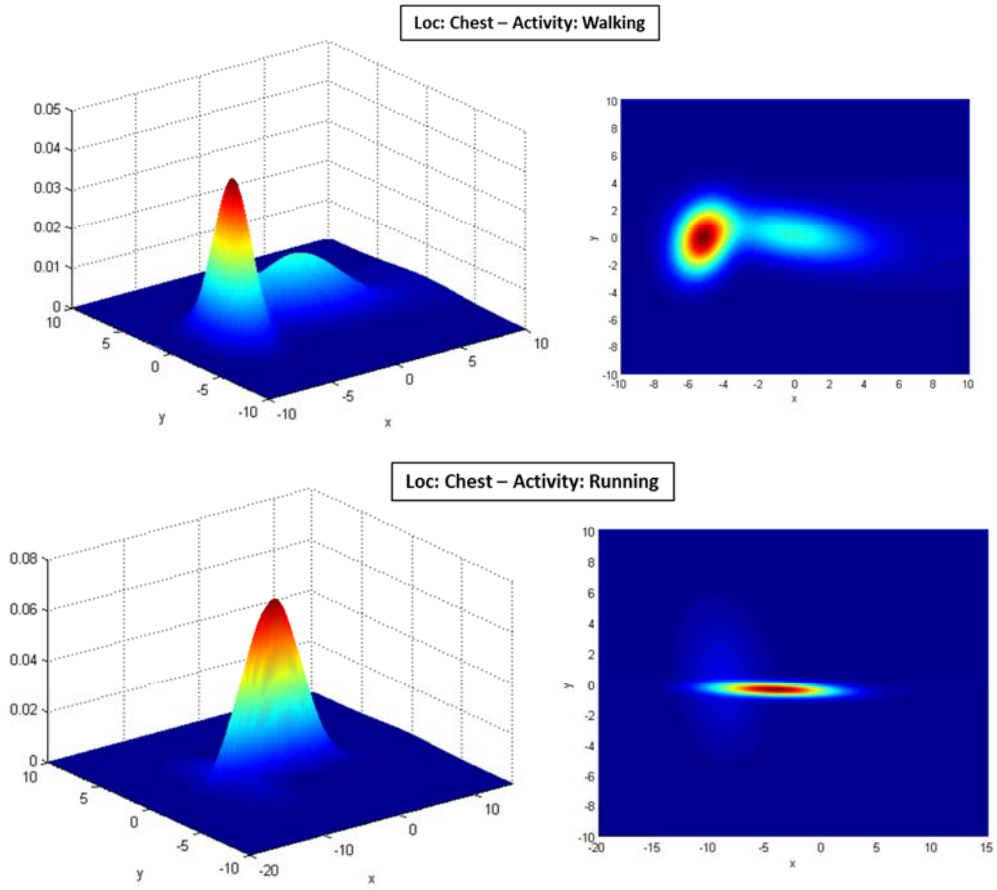

Figure 20 – Gaussian mixture models of walking and running activities estimated with two principal components.

2.7 Classification

The information provided by the statistical model was used to cluster data according to its characteristic, the sensor location and activity type. Several classification technique have been investigated for this work, among which Naïve Bayes classifiers, and divergence metrics (Hellinger distance).

Naïve Bayes Classification

Naïve Bayes classification is an example of supervised learning with the assumption that the features are independent for a given class. Bayesian classification is based on the Bayes rule for conditional probability, and it assigns the most likely class to a give example. For two events A and B, the Bayes rule is defined as

$$Pr(A|B) = \frac{Pr(B|A)Pr(A)}{Pr(B)}$$

A random variable C is used to denote the class of an example, such that $C = i$, where $i\epsilon\{1,2,\dots M\}$ and M is the number of models or elements present in the dictionary. Then, for a given discriminant function g_i, the classifier can be generally described as

$$h(\boldsymbol{x}) = \arg \max_{i\epsilon\{1,2,\dots M\}} g_i(\boldsymbol{x}) \equiv \{i|\forall j \neq i: g_j(\boldsymbol{x}) < g_i(\boldsymbol{x})\}$$

For a Bayes classifier, the discriminant function is the class a-posteriori probability, defined as

$$g_i{}^B(\boldsymbol{x}) = Pr(C = i|\boldsymbol{x}) = \frac{Pr(\boldsymbol{x}|C = i)Pr(C = i)}{Pr(\boldsymbol{x})}$$

When assuming equally probable classes, $Pr(C = k) = 1/M$ and $Pr(x)$ constant, the conditional probability $Pr(x|C = k)$ remains the only term of interest. By assuming that the features are independent within a class, the conditional probability can be expressed as a product of the single conditional probabilities

$$g_k{}^{NB}(\boldsymbol{x}) = Pr(\boldsymbol{x}|C = i)Pr(C = i) \approx \prod_j Pr(x_j|C = i)Pr(C = i)$$

The above expression implies that it is possible to estimate the density of each feature separately and then take the product of the single probabilities. In our case, the quantity $Pr(x_j\,|C = i)$ is the Gaussian mixture associated with a feature set, and using the previously defined notation

$$h^{NB}(\boldsymbol{x}) = \arg \max_{i\epsilon\{1,2,\dots M\}} \left\{ \frac{1}{M} \prod_j \sum_1^{\boldsymbol{K}} w_k \, g(\boldsymbol{x}; \theta_k) \right\}$$

Hellinger Distance

The Hellinger distance is divergence measure between probability distributions. Assumed that P(x) and Q(x) are two probability distributions belonging to the same probability space, the Hellinger distance between them is defined as

$$H(P, Q) = \frac{1}{2} \int dx \left(\sqrt{P(x)} - \sqrt{Q(x)} \right)^2$$

In this work, the Hellinger distance was used to measure model divergence for the highlighted activities of Table 1. Figure 21 illustrates the process of estimation of the Hellinger distance for one-dimensional and two-dimensional Gaussian mixtures.

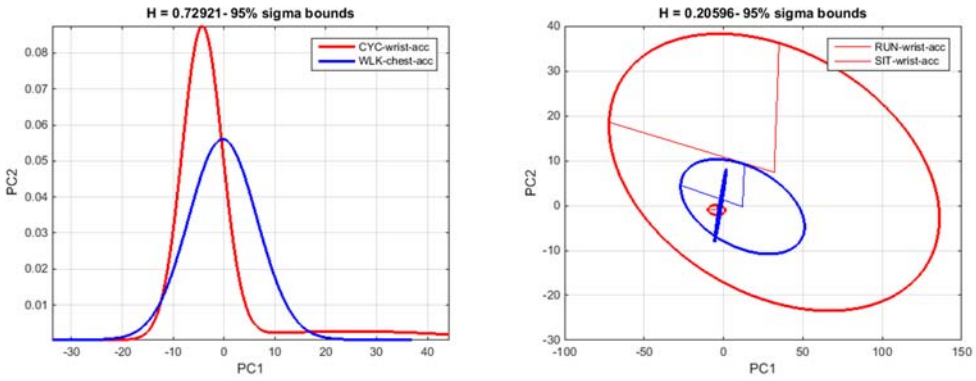

Figure 21 – Example of estimated Hellinger distance for chest sensors CYCLING-WALKING (left), and RUNNING-SITTING (right).

3. HARDWARE PROTOTYPYING

A generic analog sensor node capable of acquiring acceleration and ECG (primary inputs of interest) was developed as part of this effort. The sensor is also equipped with an IMU sensor able to provide orientation. The component of the sensor node are highlighted in Figure *22*, and are the Data Acquisition, Processing and Transmission units. The Data Display and Analysis functions are not included in the sensor itself are part of an external system. A function block diagram highlighting the components and the communication protocols used for each functionality are shown in Figure *23*. These are

- **InvenSense MPU-9150** – 9-axis Motion Tracking Inertial Measurement Unit with 3-axis MEM gyro, 3-axis MEM accelerometer, and 3-axis MEM magnetometer. This unit has a 16-bit DAC for every sensing unit.
- **TI MSP430 –** 16-bit ultra-low power microcontroller, 18MHz clock.
- **TI ADS1293 –** Low power, 3 channel, 24-bit analog front-end biopotential measurement unit with 25.6 ksps maximum bandwidth
- **TI CC2538 –** 2.4GHz IEEE 862.15.4-2006 System-on-a-chip wireless microcontroller

The firmware for the system prototype was developed using the Contiki[3] open source OS, and embedded Real Time OS that provides low overhead, a quality network stack and it is optimized for very low power consumption.

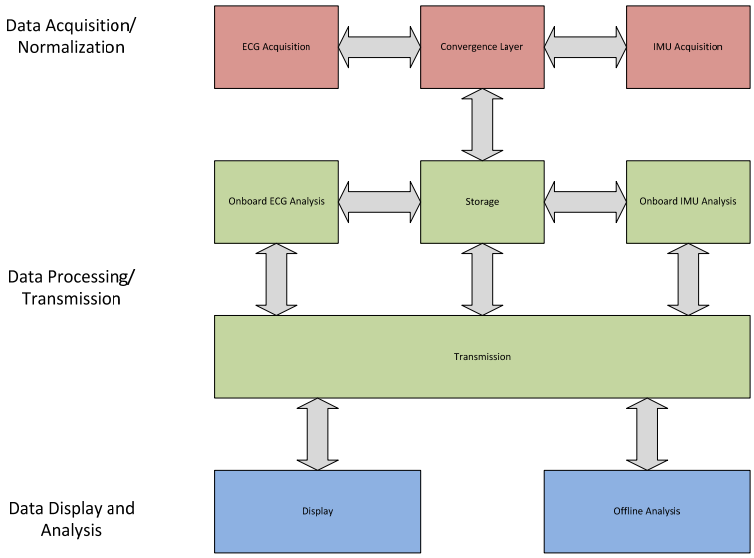

Figure 22 – Generic block diagram of sensor node highlighting major system components.

[3] http://www.contiki-os.org/

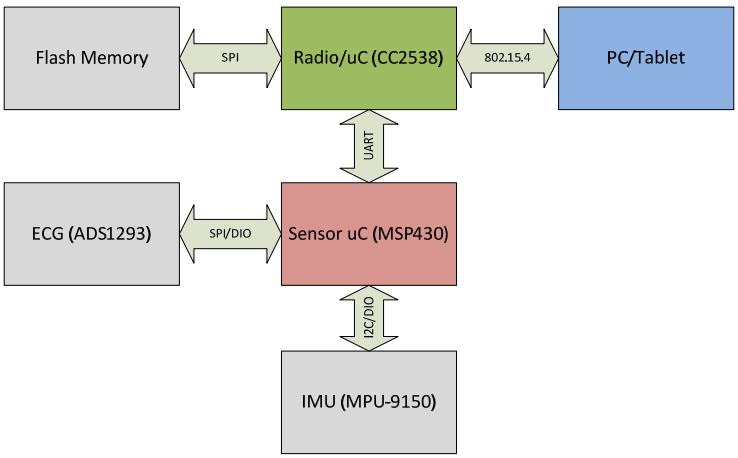

Figure 23 – Functional block diagram.

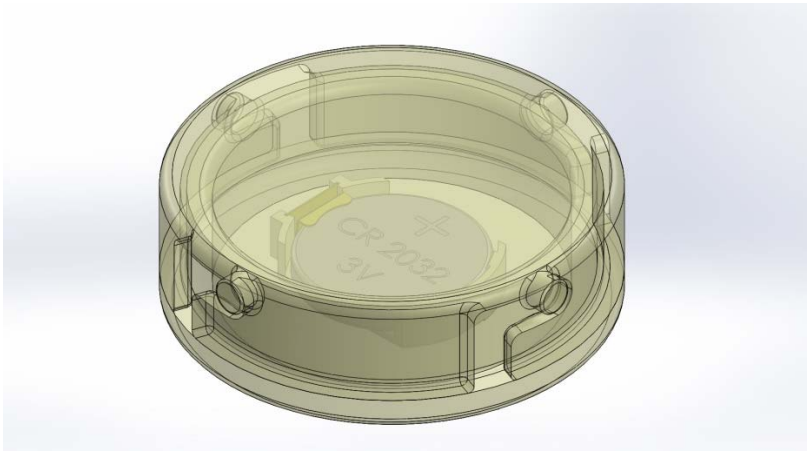

Figure 24 - Prototype enclosure for the ECG/IMU node.

An example of the CAD design for the ECG/IMU node is shown in Figure *24*. Based on this CAD, a 3D printed enclosure was manufactured and used to contain the electronics. Figure *25* shows the CAD drawing of the circular ECG/IMU node along with a booster battery pack mounted at approximately center mass on a shoulder harness. Figure *26* shows a picture of the sensor node board, with standard ECG lead connected in black, red and white, while Figure *27* shows an example of GTRI researcher wearing the sensor node prototype using a shoulder harness. This solution was chosen as a demonstration only, and it is not intended to limit its usage.

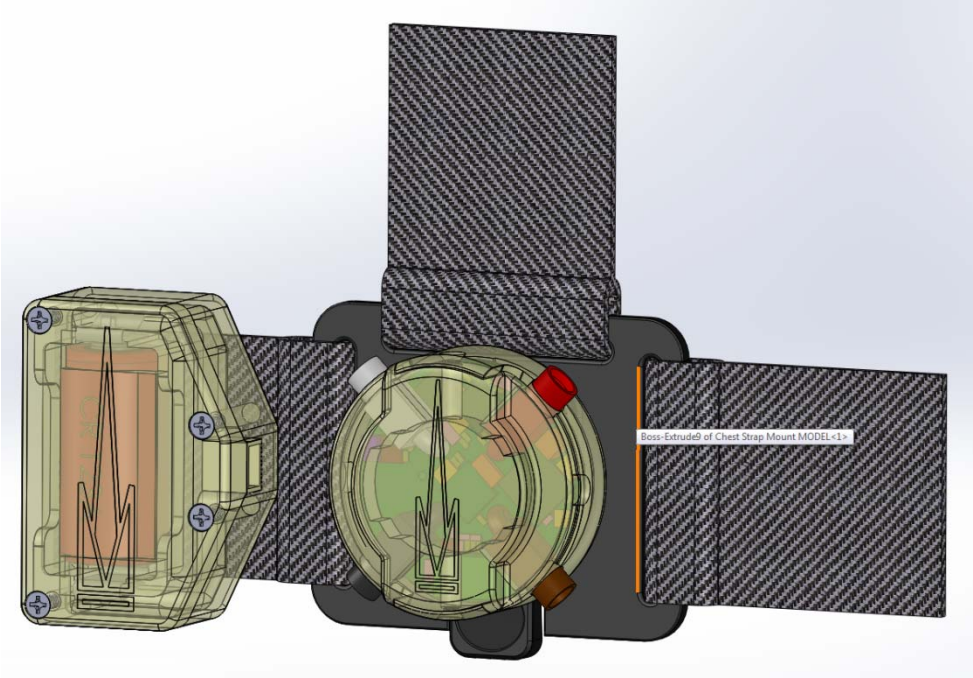

Figure 25 - 3D CAD drawing of the 3D printed enclosure and a booster battery pack mounted at approximately at the center mass on a shoulder harness.

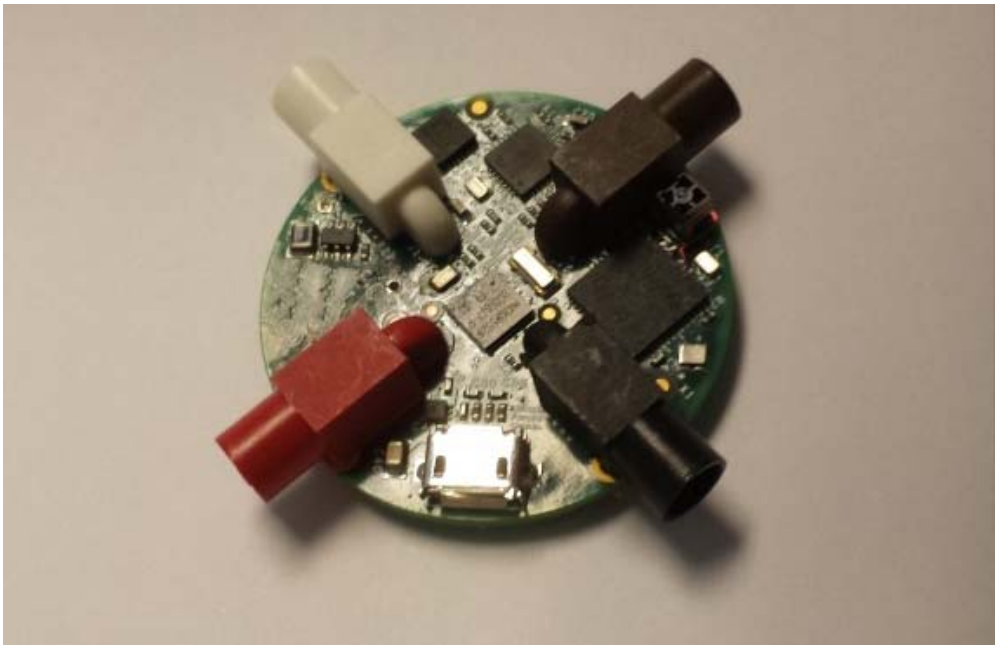

Figure 26 – Picture detailing the sensor node main board. In red, white and black are visible the standard ECG lead connectors.

Figure 27 – Picture of researcher wearing the sensor node prototype and using a commercially available harness system.

4. RESULTS AND DISCUSSION

4.1 Validation on PAMAP2 Dataset

Data from the PAMAP2 database was used to build the dictionary of basic activity of *Sitting (SIT)*, *Standing (STD)*, *Lying (LNG)*, *Walking (WLK)*, *Running (RUN)* and *Cycling* (CYC), using the algorithm described above. Self-validation was performed on the collection of model using a randomly chosen datasets for each activity type and for each sensor location. A description of the class labels used in the self-validation is shown in Table 3. Classification was done using the Hellinger distance defined between Gaussian Mixture models, and the most likely label was chosen as the one that maximizes the Hellinger distance over the entire label set. Summary of the average results are shown in Figure *28* through Figure *33*. An average classification rate is of 72% was obtained for the cross validation.

A brief analysis on the results is presented in the following:

- **CYCLYNG (CYC)**. Results are shown in Figure 28, where activity at the wrist and ankle are correctly classified.
- **LYING (LYN)**. Results are shown in Figure 29, where no correct classification is obtained.
- **RUNNING (RUN)**. Results are shown in Figure 30, where correct labels are assigned for each location.
- **SITTING (SIT)**. Results are shown in Figure 31, where correct labels are assigned for the chest and wrist locations, while the ankle location is misclassified as STD-chest.
- **STANDING (STD)**. Results are shown in Figure 32, where correct labels are assigned for each location.
- **WALKING (WLK)**. Results are shown in Figure 33Figure 32, where correct labels are assigned for each location.

TABLE 3– CLASS LABELS USED FOR THE SELF-VALIDATION.

1	**CYC** ankle	**10**	**SIT** ankle
2	**CYC** chest	**11**	**SIT** chest
3	**CYC** wrist	**12**	**SIT** wrist
4	**LNG** ankle	**13**	**STD** ankle
5	**LNG** chest	**14**	**STD** chest
6	**LNG** wrist	**15**	**STD** wrist
7	**RUN** ankle	**16**	**WLK** ankle
8	**RUN** chest	**17**	**WLK** chest
9	**RUN** wrist	**18**	**WLK** wrist

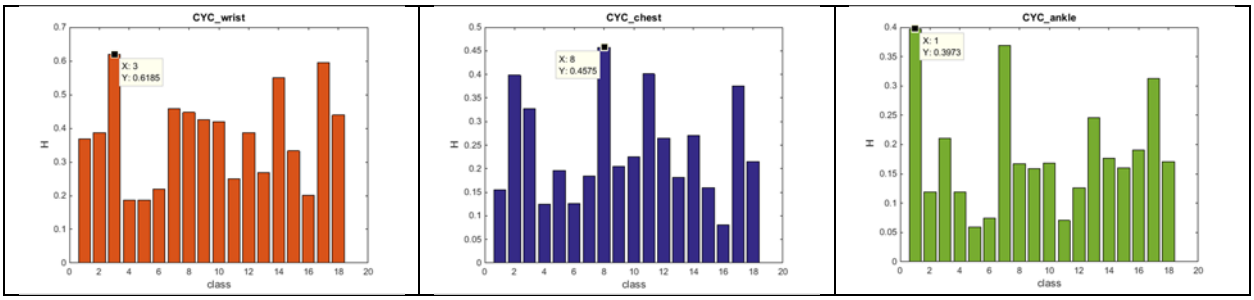

Figure 28 – Self-validation for the activity: CYCLING. Correct labels are selected for the activity recorded at the wrist and ankle, while the chest data was not correctly classified.

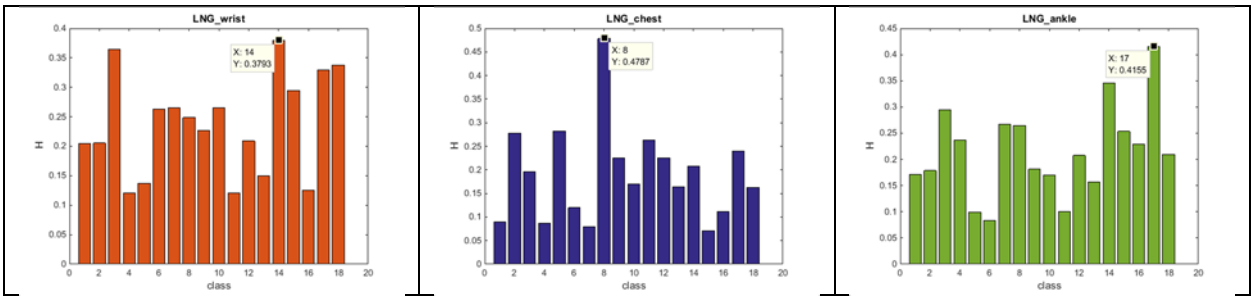

Figure 29 – Self-validation for the activity: LYING. No correct classification is obtained in this case.

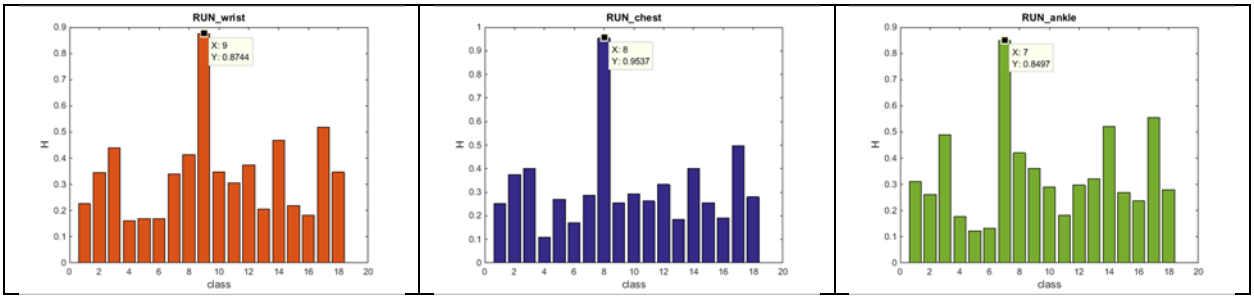

Figure 30 – Self-validation for the activity: RUNNING. Correct labels are assigned for each location.

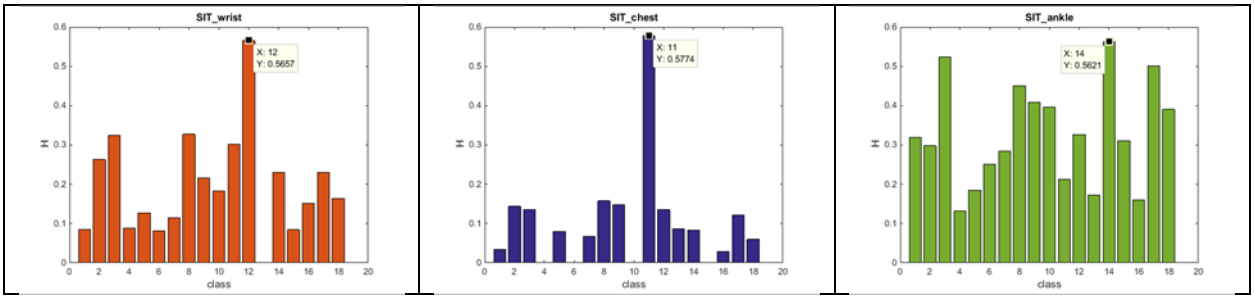

Figure 31 – Self-validation for the activity: SITTING. Correct labels are assigned for the chest and wrist locations, while the ankle location is misclassified as STD-chest.

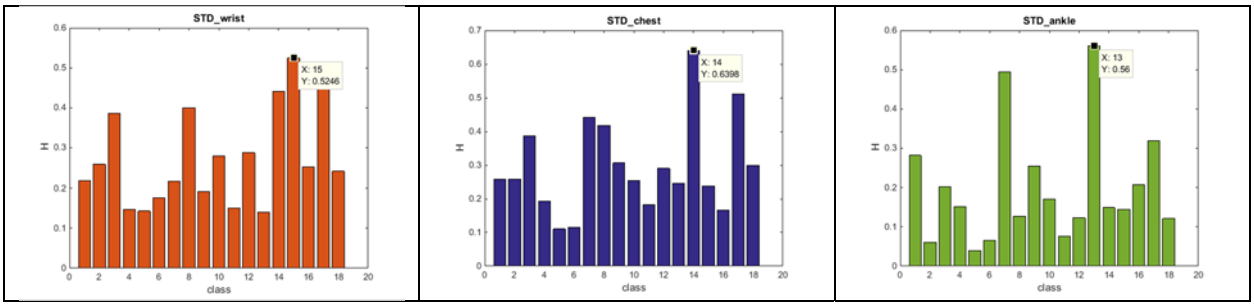

Figure 32 – Self-validation for the activity: STANDING. Correct labels are assigned for each location.

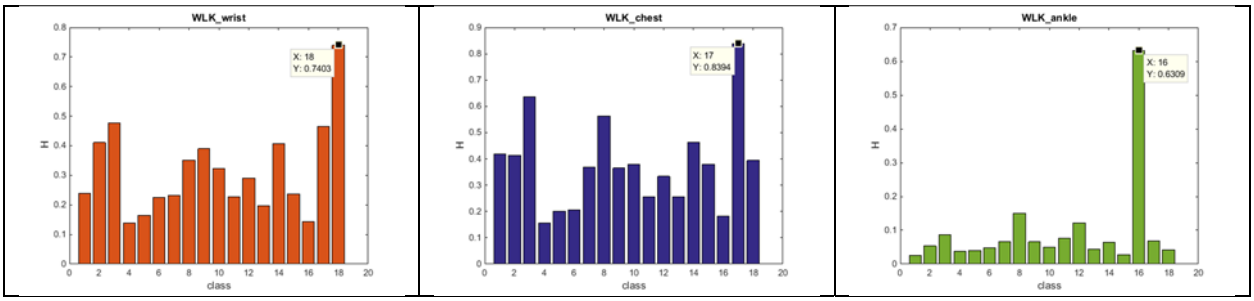

Figure 33 – Self-validation for the activity: WALKING. Correct labels are assigned for each location.

4.2 Observations on laboratory acquired data

Gaussian modeling and classification was also applied to data acquired in the laboratory for controlled conditions. For this purpose, the Shimmer wearable sensor system was employed, and data from three locations on the body were collected to match the same locations of the PAMAP2 data. Here, data was acquired at a high sampling rate of 512Hz. The researchers wearing the system were then instructed to complete a routine that comprised of a preparation and warming up session, walking at a moderate pace, running at a medium pace followed by a cooling down phase. The exercise is always completed by three jumps, representing a common denominator for the data. This was done because datasets were not synchronize among each other and there was the need to mark clearly the end of the exercise routine. Acceleration and rotational velocity was acquired at each node, and each node acquired data independently of each other; ECG was acquired by the chest sensor. An example of acceleration trace recorded at the chest can be seen in Figure *34*, while an extract of low and high intensity activity is shown in Figure *35*.

Classification results are shown in Figure *36* and Figure *37*. These plots show the strength and limitation of the two approaches. The Naïve Bayes classifier appears to work better for low intensity activities, which can be compared to a fast pace walk or slow run. In Figure *36* (left), the highest score is associated with class 16, which corresponds to walking. The score associated with the sensor at the ankle does not appear to contribute much to the results, while the periodic motion of chest and arm is most likely driving the classifier. This is still the case for the higher intensity activity, which corresponds to a medium pace run, but more uncertainty can be observed, mostly with the high score of class 11, 12 and 14 corresponding to *SIT* and *STD*.

Results for the Hellinger classifier are shown in Figure *37*. Here, although the selection of the correct class labels is not immediate due to the high H values across classes, decision on the correct labels can still be achieved. The maximum and second maximum of both graphs in Figure *37* results in

labels *WLK* and *RUN*. This is clear from the H value associated with class 7 and 8, and 17 for the low intensity activity and class 8, 17 and 18 for the high intensity activity.

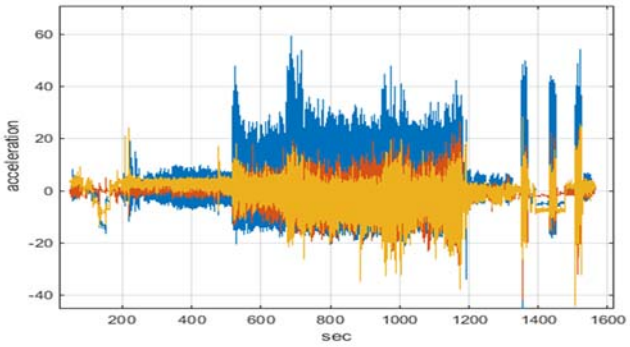

Figure 34 – Example of acceleration trace recorded for a complex activity, recorded at the chest.

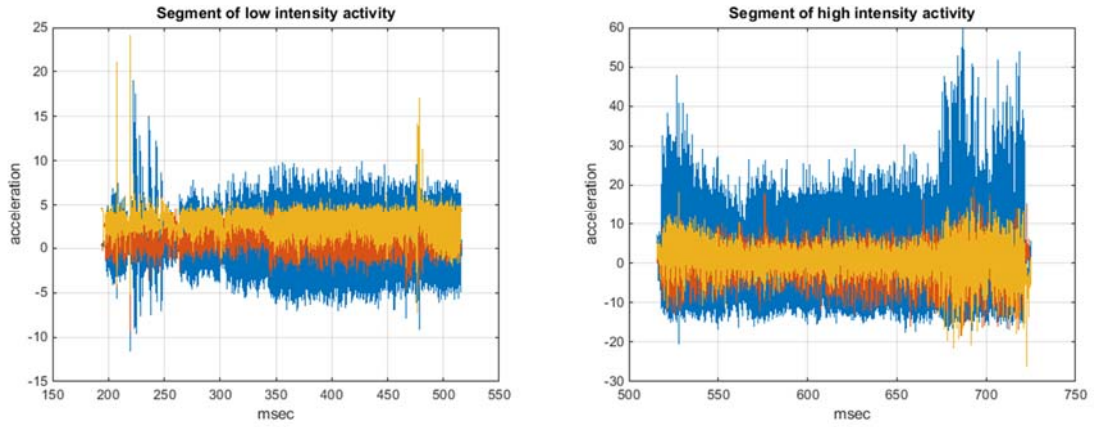

Figure 35 – Example of acceleration for low intensity activity (left) and high intensity activity (right)

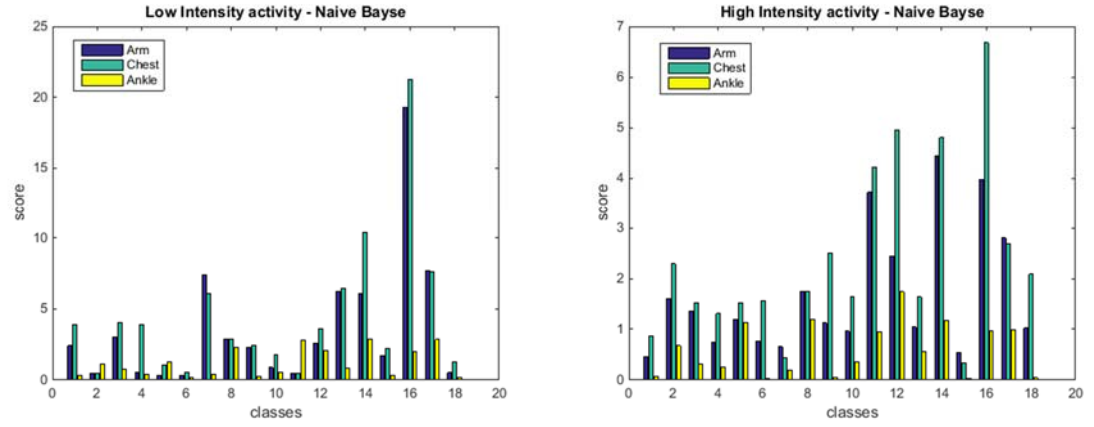

Figure 36 – Classification results for Naïve Bayes classifier.

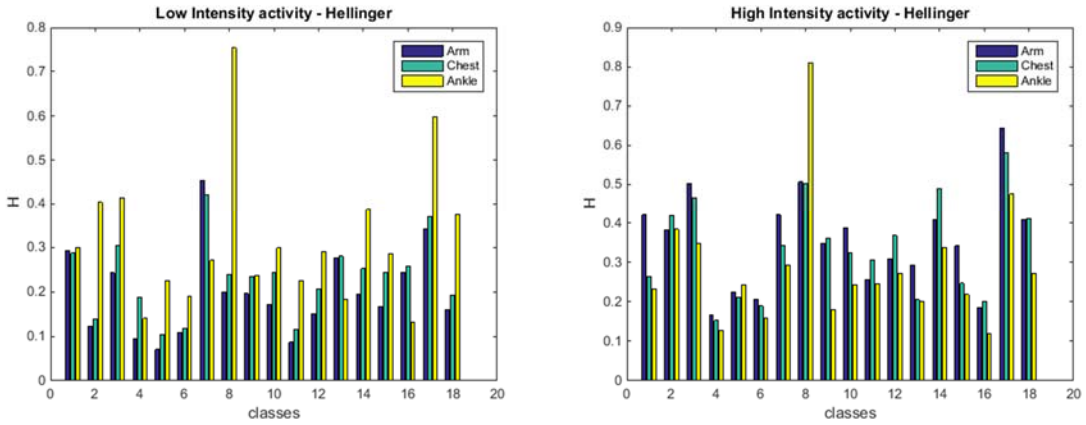

Figure 37 – Classification results for Hellinger distance classifier.

5. CODE DEVELOPMENT

The algorithm development and code generation was entirely done in Matlab®[4], and was organize in three main use-case scenarios. These scenarios are descried as following

A. Model Training: newly acquired activity data is pre-processed, segmented and features are computed. These features are then used to compute the statistical models used later for comparison and evaluation of new data.

B. Model Evaluation: a newly acquired dataset is processed and its statistical model is then compared with stored models. A label is assigned at the end of this phase

C. Model Comparison: two newly acquired dataset are processed, modeled and cross-compared. This procedure will provide a measurable alignment between two dataset, computed as Hellinger divergence between respective models

Figure *38* to Figure *40* show a schematic representation of the use-case scenarios described above. In the contest of the project, use-case **A** was used to generate a reference dataset from the PAMPA2 data, once it is correctly preprocessed. Subsequently, use-case scenario **B** was used to evaluate a new model towards the known database of models, and use-case **C** was used to compare two model between each other.

[4] https://www.mathworks.com/

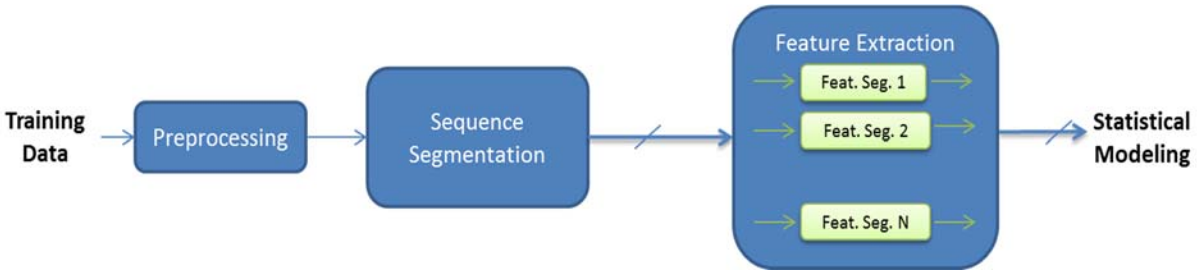

Figure 38 - Schematic representation of Model Training use-case scenario.

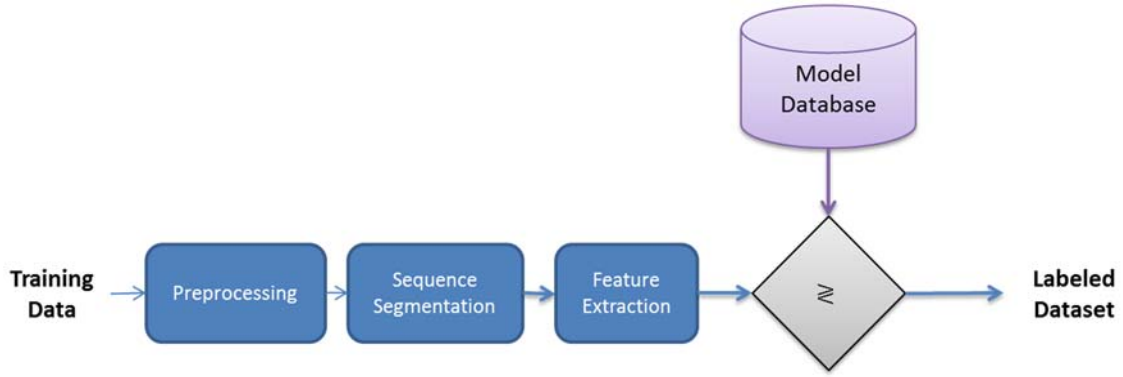

Figure 39 - Schematic representation of Model Training use-case scenario.

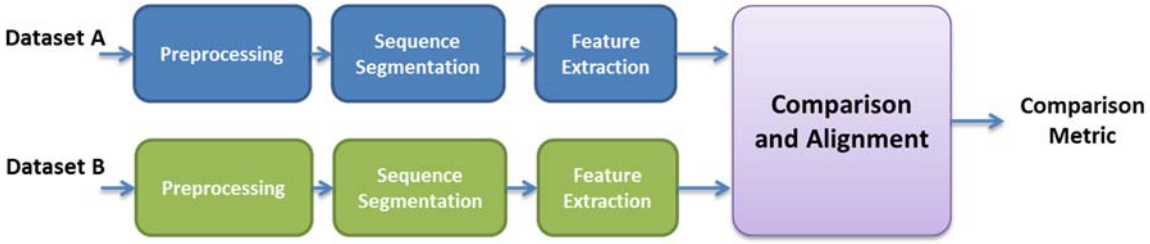

Figure 40 - – Schematic representation of Model Comparison use-case scenario.

During the course of the project, several interfaces aimed at facilitating the interaction with the code were developed. To facilitate the segmentation of complex datasets, a GUI that allow the user to select the desired breaking points was designed. The segmentation GUI is modal, and allows the user to decide is the segmentation is necessary or not. An example of the modal GUI is shown in Figure *41*, where the acceleration of the chest sensor is display for allowing the user to visually determine the compactness of the data. If segmentation is chosen, the user proceeds to a second GUI, where flexible breakpoints can be overlapped to the time trace, selecting the intervals that will define the data segments. This process is shown in Figure *42*, where a green and red bar are visible. When a bar is first added, it appears red in color, meaning that it can still be moved (by dragging) to the desired location. In the moment the bar is released, the software fixes its location, recording it in the list on the right side of Figure *42*. The segment then cannot be moved anymore, and the user can proceed to add a new segment if desired. If a mistake is made, the user can use the reset button and restart the process. In this way, the previous selected segments will be

discarded. An important option is the possibility to discard the first and last segment of the data. This is often useful for long dataset, where the data at the beginning and the end is often not desired.

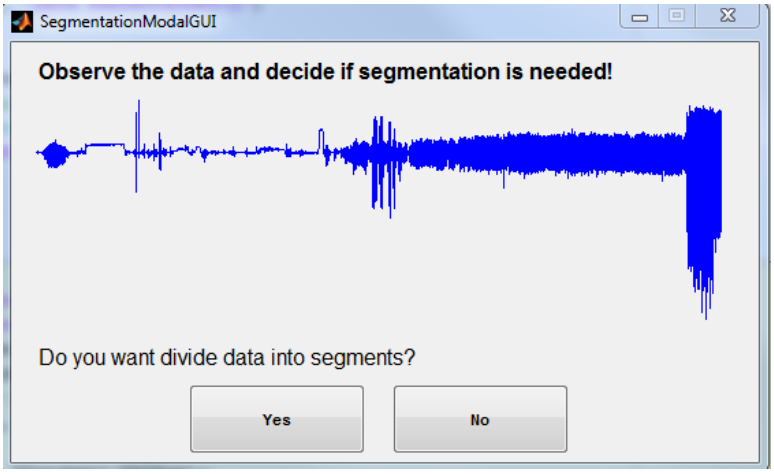

Figure 41 – Modal segmentation GUI.

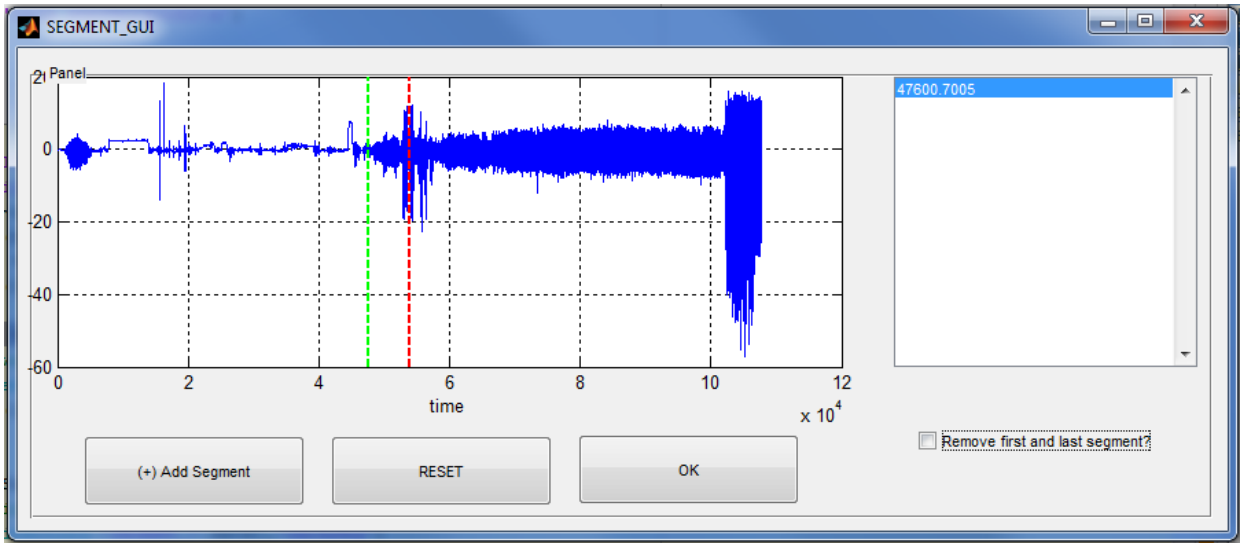

Figure 42 – Segmentation GUI details.

Another important addition to the software is the implementation of the Data Explorer and Labeling GUI. This interface is needed in the supervised learning process, where each data segment is labeled accordingly, and the model associated with it is recorded and added to the model database. A view of the Data Explorer and Labeling GUI is shown in Figure *43*, where several panels are highlighted. A description for each panel is provided in the following:

Panel 1. This panel contains the information about the dataset, and three dropdown menus for the selection of the trace of interest. By choosing the location (chest, arm, or ankle), the type of signal (acceleration, ECG, and rotational velocity) and the segment number, the use can explore the entire dataset. Only the first channel of each sensor is displayed in the plot. The LOAD button allows the user to load a new dataset, providing the option for this GUI to be used as a stand-alone product.

Panel 2. When a Location/Type/Segment combination is selected, the software loads the model associated with the data, which is previously computed and stored in memory. The precise information about the Gaussian Mixture Model is displayed in Panel 2, while the model itself can be display in Panel 3.

Panel 3. This panel displays the model associated with the data selected on Panel 1. Models that can be display are one- and two-dimensional models, while higher dimensional models cannot be display in a Cartesian plot. This is because model with more than two dimension require a four dimensional space. On the bottom of Panel 3 there are the axis zoom controls and a field to control the resolution of the model mesh.

Panel 4. This panel is designed to allow the user to easily label the data selected on Panel 1. When the user clicks on the text box, the software recognize that, a new label is desired and enables the element. Once a name for the label is chosen, clicking the ASSIGN Label button creates an object containing that model and associated with that label. This model is save in a dedicated directory on memory. It is also possible to reset a label for a given sensor dataset, by using the RESET Label button. This process removes the previously assigned label and allows the used to input a new label.

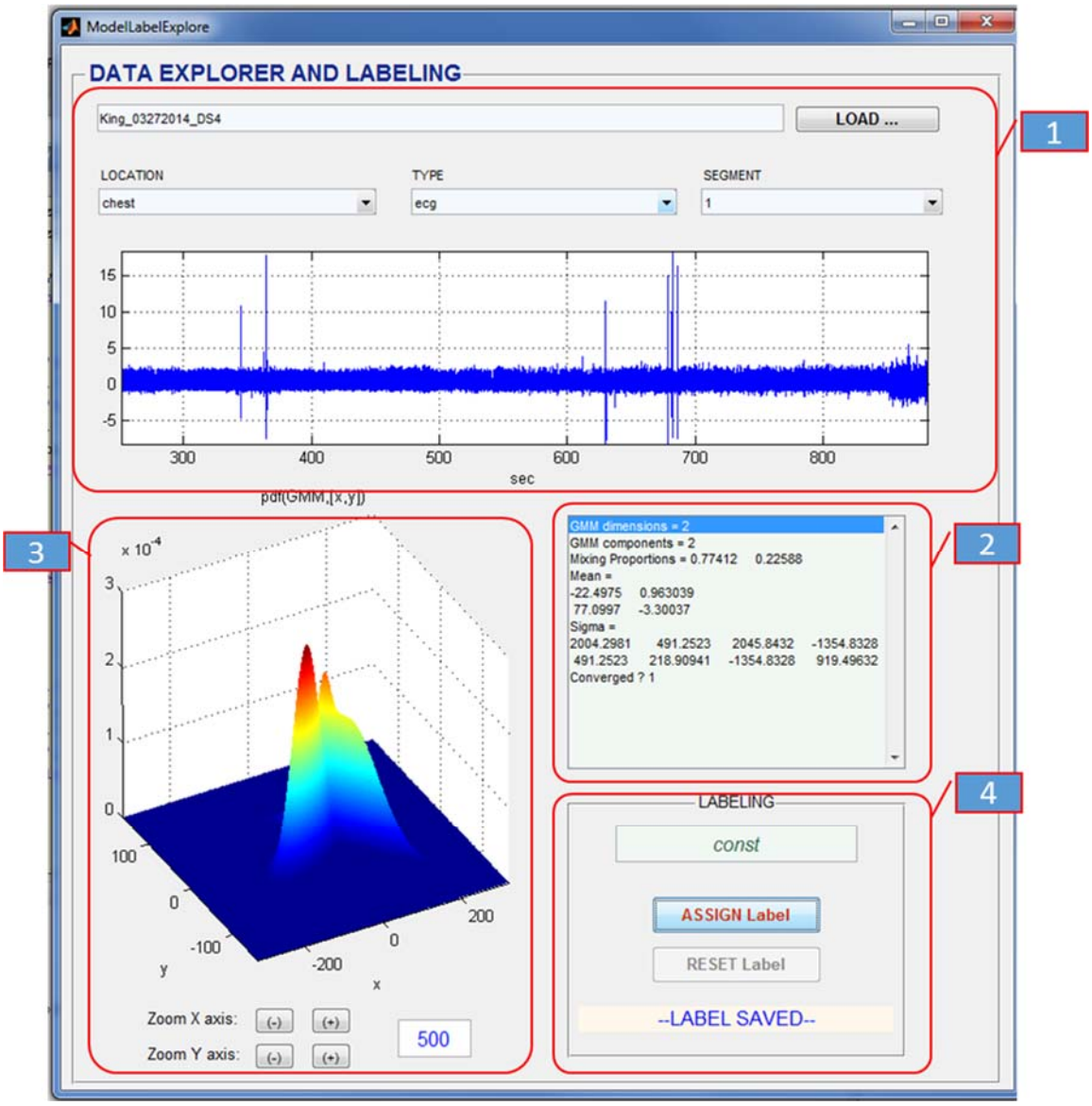

Figure 43 – Data explorer and labeling GUI with highlighted panels.

BIBLIOGRAPHY

P. Marian and T. A. Marian, “Hellinger distance as a measure of Gaussian discord,” *arXiv:1408.4477 [quant-ph]*, Aug. 2014.

A. P. Dempster, N. M. Laird, and D. B. Rubin, “Maximum Likelihood from Incomplete Data via the EM Algorithm,” *Journal of the Royal Statistical Society. Series B (Methodological)*, vol. 39, no. 1, pp. 1–38, Jan. 1977.

X. J. Xie, J. J. Xiang, and L. M. Liu, “The Application of Sensor Technology in Physical Training,” *Applied Mechanics and Materials*, vol. 336–338, pp. 144–147, Jul. 2013.

W. Zijlstra and A. L. Hof, “Assessment of spatio-temporal gait parameters from trunk accelerations during human walking,” *Gait & Posture*, vol. 18, no. 2, pp. 1–10, Oct. 2003.

W. Tao, T. Liu, R. Zheng, and H. Feng, “Gait Analysis Using Wearable Sensors,” *Sensors (Basel)*, vol. 12, no. 2, pp. 2255–2283, Feb. 2012.

W. Zijlstra, “Assessment of spatio-temporal parameters during unconstrained walking,” *Eur J Appl Physiol*, vol. 92, no. 1–2, pp. 39–44, Jun. 2004.

J. He, Y. Geng, and K. Pahlavan, “Toward Accurate Human Tracking: Modeling Time-of-Arrival for Wireless Wearable Sensors in Multipath Environment,” *IEEE Sensors Journal*, vol. 14, no. 11, pp. 3996–4006, Nov. 2014.

K. Liu, T. Liu, K. Shibata, Y. Inoue, and R. Zheng, “Novel approach to ambulatory assessment of human segmental orientation on a wearable sensor system,” *Journal of Biomechanics*, vol. 42, no. 16, pp. 2747–2752, Dec. 2009.

L. A. Schwarz, D. Mateus, and N. Navab, “Recognizing multiple human activities and tracking full-body pose in unconstrained environments,” *Pattern Recognition*, vol. 45, no. 1, pp. 11–23, Jan. 2012.

K. Altun, B. Barshan, and O. Tunçel, “Comparative study on classifying human activities with miniature inertial and magnetic sensors,” *Pattern Recognition*, vol. 43, no. 10, pp. 3605–3620, Oct. 2010.

J. J. Verbeek, N. Vlassis, and B. Kröse, “Efficient Greedy Learning of Gaussian Mixture Models,” *Neural Computation*, vol. 15, no. 2, pp. 469–485, Feb. 2003.

K. Dragomiretskiy and D. Zosso, “Variational Mode Decomposition,” *IEEE Transactions on Signal Processing*, vol. 62, no. 3, pp. 531–544, Feb. 2014.

I. Cleland, B. Kikhia, C. Nugent, A. Boytsov, J. Hallberg, K. Synnes, S. McClean, and D. Finlay, “Optimal Placement of Accelerometers for the Detection of Everyday Activities,” *Sensors*, vol. 13, no. 7, pp. 9183–9200, Jul. 2013.

S. Chernbumroong, A. S. Atkins, and H. Yu, “Activity classification using a single wrist-worn accelerometer,” in 2011 5th International Conference on Software, Knowledge Information, Industrial Management and Applications (SKIMA), 2011, pp. 1–6.

L. Oudre, J. Jakubowicz, P. Bianchi, and C. Simon, “Classification of Periodic Activities Using the Wasserstein Distance,” *IEEE Transactions on Biomedical Engineering*, vol. 59, no. 6, pp. 1610–1619, Jun. 2012.

J. Parkka, M. Ermes, P. Korpipaa, J. Mantyjarvi, J. Peltola, and I. Korhonen, “Activity classification using realistic data from wearable sensors,” *IEEE Transactions on Information Technology in Biomedicine*, vol. 10, no. 1, pp. 119–128, Jan. 2006.s

M. Zhang and A. A. Sawchuk, “A Feature Selection-based Framework for Human Activity Recognition Using Wearable Multimodal Sensors,” in *Proceedings of the 6th International Conference on Body Area Networks*, ICST, Brussels, Belgium, Belgium, 2011, pp. 92–98.